www.sciencemag.org/cgi/content/full/science.aad2646/DC1

Supplementary Materials for

Microbial community assembly and metabolic function during mammalian corpse decomposition

Jessica L. Metcalf,* Zhenjiang Zech Xu, Sophie Weiss, Simon Lax, Will Van Treuren, Embriette R. Hyde, Se Jin Song, Amnon Amir, Peter Larsen, Naseer Sangwan, Daniel Haarmann, Greg C. Humphrey, Gail Ackermann, Luke R. Thompson, Christian Lauber, Alexander Bibat, Catherine Nicholas, Matthew J. Gebert, Joseph F. Petrosino, Sasha C. Reed, Jack A. Gilbert, Aaron M. Lynne, Sibyl R. Bucheli, David O. Carter, Rob Knight*

*Corresponding author. E-mail: rob.knight@ucsd.edu (R.K.); jessica.metcalf@colorado.edu (J.L.M.)

Published 10 December 2015 on *Science* Express
DOI: 10.1126/science.aad2646

This PDF file includes:

Other Supplementary Material for this manuscript includes the following:
(available at www.sciencemag.org/cgi/content/full/science.aad2646/DC1)

Tables S18 and S19 (Excel files)

Materials and Methods

We compared microbiome results from laboratory (mice) and field (human) experiments to answer basic questions about the succession of microbes during decomposition and their potential for forensic science.

Laboratory Experiment - Mouse Model System

We characterized archaeal, bacterial and microbial eukaryotic decomposer community succession by studying the decomposition of a model mammal organism, *Mus musculus*, in a controlled laboratory setting. By using a mouse model, we were able to perform a highly replicated experiment with destructive sampling that enabled us to sample both the surface and interior of each corpse at each sampling time point. Importantly, this approach allowed us to sample the abdominal cavity prior to natural corpse rupture, and thus, our data address forensic hypotheses that abdominal microbes are likely important in corpse decomposition (*10*).

The decomposition of mouse carcasses was conducted at the University of Colorado Transgenic Mouse Facility. This facility is located on the University of Colorado Boulder campus and occupied a small room dedicated solely to the experiment with little foot traffic. The temperature of this room was maintained between 20 °C – 21°C (68 °F – 70 °F). We allowed 120 mice to decompose on three contrasting soil types collected from short grass prairie, subalpine forest, and desert environments (**fig. S1**). The biological and chemical characteristics of these three soils differed in many ways, including dominant plant species, pH, carbon:nitrogen ratio, total carbon and total nitrogen. Shortgrass prairie soils were collected from Shortgrass Steppe Long Term Ecological Research site in northern Colorado. Soils from the shortgrass prairie are likely late Holocene in age and are sandy soils derived from local sources. The plant community is dominated by the short-stature C4 grasses blue grama (*Bouteloua gracilis*) and buffalograss (*Bouteloua dactyloides*), the forb scarlet globemallow (*Sphaeralcea coccinea*), the cactus plains pricklypear (*Opuntia polyacantha*), and the dwarf shrubs prairie sagewort (*Artemisia frigida*), spreading buckwheat (*Eriogonum effusum*), rubber rabbitbrush (*Chrysothamnus nauseosus*), and broom snakeweed (*Gutierrezia sarothrae*). Subalpine forest soils were collected from University of Colorado's Mountain Research Station, which is dominated by lodgepole pine (*Pinus contorta*). Soils are derived from gneiss and schist with angular gravel, stone, very little silt and clay, and a thin organic-rich mineral horizon of ~3–12 cm in depth. The desert soils were collected from a cool desert ecosystem on the Upper Colorado Plateau near Castle Valley, UT, USA. Soils are derived from sandstone sources and are classified as sandy loam, calcareous, Rizno series. The site's vegetation is dominated by the perennial grasses *Achnatherum hymenoides* and *Pleuraphis jamesii*, the perennial shrub *Atriplex confertifolia*, and the annual invasive grass *Bromus tectorum*. At each site, soils were collected from the surface (0 cm - 10 cm depth) and sieved (4mm). Soils were homogenized with a large shovel, and ~600g of soil was added to each "grave", which was a clean polypropylene (Rack, Empty; Fisherbrand; SureOne; For standard tip volume 1250 µL, 02-707-443). Water Holding Capacity (WHC) was estimated for each soil type, and calibrated to ~50% WHC. Water was mixed in box and boxes left to sit for ~1 week so that the soil communities could equilibrate. The total

weight of each box was checked daily (or so) to monitor water loss and water was added to replace lost water.

We used 120 female Hsd:ICR(CD-1) strain mice from Harlan Laboratories. Mice were acclimated to a conventional facility at the University of Colorado, MCDB Animal Care Facility. They were raised in Specific Pathogen Free conditions prior to arrival in the facility. Mice were humanely sacrificed using CO_2 gas followed by cervical dislocation. Fecal samples from mice were opportunistically sampled at the start of the experiment (prior to sacrifice). Mice were placed on their right side on top of soil in a clean Tupperware-type container with a small hole drilled into each side above soil level to prevent anoxia. Approximately six individual mouse graves were placed in an autoclavable polycarbonate Nalgene rat cage with a microfilter top to exclude insects. Individual mouse graves were grouped into the secondary containers by treatment (soil type) to help prevent cross-contamination of microbial soil communities. To regulate the loss of water from the soils in the dry Colorado climate, humidity in the polycarbonate cages was kept high by lining the cages with soaked lab bench paper.

We used sterile swabs (BD BBL™ CultureSwab™, Becton Dickinson, USA) to sample the soil-free surface of the skin on the head and torso of each mouse while it was still in its aboveground position on the gravesoil (see **fig. S1**). Once mouse skin sites were sampled, the mouse was removed from the grave box, and ~10 g of soil was collected using a sterile spoon from the area underneath where the mouse was decomposing, and deposited into a new Ziplock bag. Soil in the bag was swabbed for DNA extraction, and remaining soils were used for soil chemistry measurements (described below). On a clean lab bench, an incision was made to access the abdomen, and the cavity was swabbed (outside of the intestines and stomach as long as they were intact). Next, the cecum was removed and placed in a 1.5 ml Eppendorf tube, and later homogenized with a swab for DNA extraction. Mice decomposed for 71 days and 5 mice were sampled from each soil type 8 times over the experiment with sampling events occurring more frequently (~every 3 days) over the first two weeks (**fig. S1**). The cecum was sampled until it was no longer visibly recognizable ~day 14 - day 29. For one pre-rupture (day 3) and one post-rupture time point (day 29), we resampled soils three additional times after the mouse cadaver was removed – at 10, 20, and 30 days postmortem. For each soil sample, we suspended 1 g of each soil sample in 5 ml of deionized water and measured pH using an Orion 3 Star benchtop pH meter (Thermo Scientific, USA). For each sample, triplicate pH measurements were averaged for a final pH estimate for each sample.

For the laboratory experiment, we also measured the concentration of total carbon, total nitrogen, ammonia, and nitrate in all soil samples. For nitrate and ammonia extractions, soils were amended with 2M KCl immediately following harvest by weighing 5 g wet soil, adding 2M KCl, shaking for 1 hour at 200 rpm, allowing the samples to settle for 1 hour after shaking, and vacuum filtering using Whatman No. 1 filter papers. These extracts were then analyzed at the Colorado State University Soil, Water, and Plant Testing Laboratory (http://www.soiltestinglab.colostate.edu). Another soil subsample was collected, dried at 60 °C for 48 h, sieved (2 mm), ground, and

analyzed for total carbon and nitrogen content using an elemental analyzer (ECS 4010; Costech Analytical, Valencia, CA, USA) at the University of Colorado's Arid Lands Ecology Laboratory. We followed the soil chemistry protocols available at http://www.colorado.edu/eeb/facultysites/barger/protocols.html.

Field experiments were conducted at the Sam Houston State University Southeast Texas Applied Forensic Science Facility (STAFS). The STAFS facility is approximately 5 km north of Huntsville, Texas (Walker County) and is an outdoor, two-acre area fenced off within the larger 247 acres of The Center for Biological Field Studies located in the Pineywoods ecoregion characterized by a humid and subtropical climate and a sparse forest covering of pine trees and a ground covering of herbaceous plants. We sampled soil and skin sites associated with human cadavers (*Homo sapiens sapiens*). Cadavers are donated to the Southeast Texas Applied Forensic Science (STAFS) Facility at the Center for Biological Field Studies (CBFS) at Sam Houston State University (SHSU) as part of the willed body donation facility. Donors (or next of kin) relinquish all rights and claims regarding the body after death, making it available for teaching or scientific purposes. Donated cadavers are placed outside to decompose under natural conditions for research studies. The SHSU Institutional Review Board, the Protection of Human Subjects Committee, granted exempt status since no personal or identifiable information is collected.

We collected samples during two experiments over two winter and spring seasons. For the winter experiment two bodies were placed in the field on February 26th, 2013, and samples were collected from three skin sites (left hip, right hip, left knee) and four soil sites (next to the left hip, right hip, left knee, head). Swabs from three control soil sites (no corpse) were also collected. In the winter experiment, samples were collected daily for the first month, and then every three to four days for an additional month until April 29th, 2013. Additionally, samples were collected once a month in May, June, and July, at which point sampling was terminated. For the spring experiment, bodies were placed on 17 April 2013, and samples were collected from eight skin sites (left hip, right hip, left bicep, right bicep, left upper hip, right upper hip, groin, head) and six soil sites (next to the left hip, right hip, left armpit, right armpit, left knee, groin, head) as well as three control soil sites that were not associated with the corpse. Samples were collected every other day for the first month, and then every four days until the end of May, and then once a month in June and July.

Skin sites were sampled by non-abrasively (without breaking the skin) swabbing with a sterile cotton tipped applicator (Puritan, 25-806 1WC) or (BD BBL™ CultureSwab™, Becton Dickinson, USA). The cotton tip was removed and placed in a collection tube (VWR Sterile screw-cap cryo tube, 89004-310) containing 0.5 ml standard phosphate buffered saline (pH 7.4) and stored at -80 °C until processing for bacterial genomic DNA. Soil samples were collected from the surface using a sterile metal spatula and stored in a 15 ml sterile polypropylene centrifuge tube (VWR, 89039-666). Because the human experiments required repeated samples, we minimized the amount of soil collected at each time point (~10g), and we sampled at a depth of no more than 10 cm from the starting surface to avoid soil microbial community changes due to

soil depth. All samples were immediately frozen after collection at -20 °C. Soil was later swabbed for DNA work and the remainder of the soil was utilized for pH measurements. For each soil sample, we suspended 1g of soil in 5 ml of deionized water and measured pH using an Orion 3 Star benchtop pH meter (Thermo Scientific, USA). Triplicate pH measurements were averaged for a final pH estimate for each sample.

We collected insects associated with human cadavers on days 1 and 3 of the winter experiment at SHSU. We collected insects from the families Muscidae, Calliphoridae, Anthomyiidae and dissected out their tarsi (leg) for DNA extraction and 16S rRNA sequence generation.

For cross-experiment comparisons, we compared time point with Accumulated Degree Day (ADD) since temperatures varied across experiments, likely affecting the rate of microbial community change. Accumulated Degree Day (ADD) was calculated using a base of 0°C, where degree day (DD) = ((maximum temp + minimum temp)/2)-base temperature, ADD = DDx + DDx+1, and x = 24 hour period.

DNA Extraction and Sequence Data Generation

For all samples collected, we extracted DNA and generated 16S rRNA and 18S rRNA amplicon sequence data following the protocols recorded in Caporaso et al. (*16*) and the Earth Microbiome Project (EMP) webpage (http://www.earthmicrobiome.org/emp-standard-protocols/). These are also described in Metcalf et al. (*7*). For fly tarsi, only 16S rRNA data were generated. ITS amplicon preparation followed Bates et al. (*17*) and McGuire et al. (*18*). All amplicon sequencing except for fly tarsi samples was accomplished using the Illumina HiSeq platform at the University of Colorado Boulder Next Generation Sequencing Facility in the BioFrontiers Institute. For all samples collected on the first day of each experiment, we deeply sequenced 16S rRNA amplicons by only including 45-50 samples per lane of Hiseq 2000. Fly tarsi samples were sequenced on a Miseq at the Human Genome Sequencing Center at Baylor College of Medicine.

Sequence Data Processing and Analysis

16S rRNA amplicon processing

Using the default settings in QIIME (*19*), barcoded Illumina 16S rRNA sequences were quality filtered and demultiplexed using error-correcting Golay codes that reduce the possibility of sample mis-assignment. All sequences were 100 bp in length (read 1) with the exception of fly tarsi data, which were 250 bp in length. Fly tarsi data read 1 and 2 were merged using USEARCH v7.0.1090, allowing four mismatches and a minimum overlap of 50 bases. Merged reads are trimmed at first base with Q5. In addition, a quality filter was applied to the resulting merged reads and reads containing above 0.5 expected errors were discarded.

We classified sequence reads into Operational Taxonomic Units (OTUs) on the basis of sequence similarity using the greengenes 13_5 reference data set (link to all

reference data sets can be found at (http://qiime.org/home_static/dataFiles.html). We filtered out plant Chloroplast using filter_taxa_from_otu_table.py. We removed low abundance OTU's making up <0.0005% of reads in the total data set as recommended for Illumina generated data (*20*). Samples with less than 1000 sequences per sample were considered failures and filtered out.

18S rRNA sequence processing

Raw 18S rRNA sequence data were subjected to similar processing and demultiplexing protocols within QIIME as described above, except that a curated version of the Silva 108 database was used as the reference database (original: http://www.arb-silva.de/documentation/release-108/; Pruesse et al. (*21*), curated version available at qiime.org/home_static/dataFiles.html). Sequences not corresponding to eukaryotic 18S were removed from the dataset prior to analysis by excluding reads that failed to align to the eukaryotic portion of Silva 108 at a low similarity threshold (70% sequence similarity) with PyNAST (*22*) within QIIME. The dataset was further filtered to exclude all sequences assigned to vertebrate animals, as these likely correspond to the mouse host. We also filtered out insects and Similar to 16S data, we removed low abundance OTU's making up <0.0005% of reads in the total data set as recommended for Illumina generated data (*20*).

ITS sequence processing

We processed the ITS fungal amplicon data following methods outlined in McGuire et al. (*18*) using the QIIME pipeline in a similar way as for 16S rRNA and 18S rRNA amplicon data, except that UNITE version 09.02.2014 was used as the reference database. The reference files of untrimmed version (containing flanking LSU and SSU sequences) in the developer folder of UNITE database were used, for the reads will fail to align to the ITSx trimmed sequences. The OTUs are clustered at 97% level using close-reference picking strategy. Similar to 16S data, we removed low abundance OTU's making up <0.0005% of reads in the total data set as recommended for Illumina generated data (*20*).

Statistical Analysis of Microbiome Data

We performed the majority of our statistical analyses and visualizations using the QIIME software package (*19*), including relative abundance of taxa, and alpha and beta diversity patterns. We report the mean number of sequences per sample in each data set (16S rRNA, 18S rRNA, and ITS) for each experiment (mouse and human), as well as the levels at which these datasets were rarified for statistical analyses (**table S14**). Alpha diversity was estimated using Faith's phylogenetic diversity metric (PD) as the average across ten different rarefactions to the depths described in **table S15**. Smooth curves were fitted over abundance plots over time using the loess smooth function in the R package ggplot2 (**fig. S5**). We explored beta diversity patterns by performing principal coordinate analyses (PCoA) with phylogeny-based (UniFrac) unweighted distances. PERMANOVA and ANOSIM were used to test for significant differences between microbial communities in pre- and post-rupture samples, control soils and grave soils, contrasting soil types, and other variables (**Tables S1,3,7,9,11**). Differences in diversity levels between groups were tested using a nonparametric two sample t-test (999 Monte Carlo

permutations) through the QIIME script compare_alpha_diversity.py (**Tables S2, 4,6,8,10,12**).

Heatmap of bacterial succession in SHSU experiments

A custom matlab script was used for generation of **Fig. 1B and fig. S8**. For each OTU, The frequency data of all the skin samples from individual #4 were log transformed and combined to a single vector sorted by sampling time. This vector was then tested by scanning all possible time windows (made of at least 20 consecutive samples). If in at least one such window, the OTU had a >8 fold higher median frequency for samples in the window (compared to samples from times outside the window), it was kept for the heat map. The start time of this OTU was then defined as the first time point of the window showing the largest median frequency fold change (over all possible windows of at least 20 consecutive time points). Additionally, to remove OTUs which are not decomposers, OTUs showing a high frequency in the first timepoint were removed. Ordering of the samples was then obtained by sorting these start times. The same OTU order was then used for displaying the frequency of the same OTUs in individual #16.

Random Forest regression models

We used Random Forest regression to model the PMI as a function of the changes in OTU abundances. 10-fold cross-validation (CV) was performed to tune and evaluate the models, i.e., the input samples are partitioned into 10 subsets and models are built on 9 subsets and validated using the rest subset. This cross-validation process is then repeated 10 times, with each of the 10 subsets used exactly once as the validation data. The accuracy of models is measured as root mean squared error (RMSE). It is calculated as the standard deviation of the differences between the predicted and observed values, representing the average prediction error in the same unit of original data (in this case, days). The most parsimonious model (in order to avoid overfitting to the input training data) within one standard deviation of the optimal accuracy were chosen as the final model. Results for each amplicon data set can be found in **fig. S6**.

We also tested how well our regression model built on one experiment can be generalized to another experiment. We built a random forest model using the OTU table from soil type mouse data set (including abdominal, skin, and soils), and used it to predict the PMI for samples in the other soil types (**fig. S7**). We built the random forest model using the OTU table from the human decomposition in the winter season and applied it to predict the PMI of the other decomposition in spring season (**Fig. 1C**). To account for the temperature difference between the two season, given that temperature dramatically impacts microorganism growth, we used ADD (Accumulated Degree Day) instead of days as the measure of PMI. To guide and justify the necessary sampling frequency for accurate PMI prediction, we did regression analyses on samples either collected every day, every 2 days, every 3 days, or every 4 days. The RMSE were plotted for each scheme of sampling frequencies (**fig. S15**).

Shared important regression features (OTUs) across experiments

To investigate whether the decomposer community was shared across environments and experiments we performed bootstrapping experiments. For each pairwise experiment

(mouse decomposition, April human decomposition and February human decomposition) and each ADD, we selected the 100 most predictive features for the PMI regression. We then asked, for each pairwise combination of experiments, how many of those features were shared at a given ADD. The colored lines in **Fig. 1D** indicate the number of shared important features between each pair of experiments (column label) and for each marker gene (row label). The gray lines indicate bootstrapping controls where we randomly selected 100 features from each experiment and each ADD, and plotted the number of shared features. In all cases, the number of shared features is significantly higher (especially as ADD increases) than the randomly selected bootstraps. 100 bootstraps were performed for each ADD and error bars indicate standard deviation. We also generated this graph using days, ADD 0, ADD 4, ADD 5, and ADD 6 and the patterns remained regardless of time-scale selected.

Dynamic Bayesian Networks

The Dynamic Bayesian Networks (DBN) in **Fig. 2A**, which models interactions between bacterial taxa during mouse decomposition, was created by collapsing the 16S OTU table to order and filtering out taxa that did not meet one of the following criteria: an average abundance of less than 0.5% or a maximum abundance of greater than 5%. All data normalized such that abundances from a single observation sum to 100. Bayesian Network Inference was calculated using BANJO (http://www.cs.duke.edu/~amink/software/banjo/) (*23*). Analysis conditions: discretization = 5 intervals; max parents=5; min lag = 0; max lag = 1; using Greedy search algorithm. In all networks, soil is significantly (calculated as hypergeometric distribution, significant at a p-value <0.01) more likely to be a source of bacteria for colonization of mouse (p-values: Forest: 0.000096; Desert: 0.00017; Grassland: 0.00076). Mouse was, in all cases, more frequently a sink than a source for bacterial colonization, but that increased frequency was not statistically significant. The soil source bacteria found by DBN analysis were significantly (calculated as hypergeometric distribution, significant at a p-value <0.05) enriched for specific bacteria taxa, though the specific taxa differed by soil type **(table S16).**

Defining the bacterial decomposer community using DESeq2

We defined the decomposer community by estimating the OTUs that became significantly differentially abundant in the post-rupture communities using DESeq2 (*24, 25*) on rarefied data with Benjamini & Hochberg FDR correction. Since there were no systematic differences in library sizes between sample categories, and the rarefying depth (11000 for 16S rRNA) was relatively high, we used DESeq2 to increase detection sensitivity, especially for rare OTUs. For summarized taxa tables, we used the nonparametric Kruskal-Wallis test, after removing OTUs that did not occur in more than 10% of samples. We compared shared taxa in these communities with Venn diagrams (**figs S16-S17**).

Decomposers detected in deeply sequenced 16S rRNA data

Samples deeply sequenced for 16S rRNA were rarefied to 250,000 sequences per sample, and OTUs not occurring in greater than one sample were removed. The remaining deeply sequenced OTUs were counted as present at day 1 if they were present

at least once in the sample. 'Decomposer taxa' were defined as those that significantly increased in post-rupture samples by DESeq2. The proportion and relative abundance of decomposer taxa present at day 1 was then calculated (**Fig. 2B**). We report standard error for the proportion of decomposer OTUs detected in each day 1 environment. We calculated 3.4e-05 as the median relative abundance of the decomposer OTUs at T0 for all environments. We compared the proportion of decomposers detected in day 1 abdominal, soils, and skin samples using Mann-Whitney U test.

Inter-domain Bayesian networks

The network in **Fig. 3A** modeled interactions between bacterial and eukaryotic taxonomic orders with environmental factors, and was created as follows. 16S data were collapsed to the level of order and all orders not containing at least 1000 reads were discarded, with all samples then rarified to an even depth of 20,000 reads. ITS data were similarly collapsed to order and all orders not containing at least 500 reads were discarded, with samples then rarified to an even depth of 5000 reads per sample. Because only 2 major non-fungal eukaryotic orders were detected through 18S, and those primers produced very few reads any reads in early time points, Discicristata and Nematoda were treated as dummy variables with an abundance of 0 for time points 0-4 and 1 for 5-7. The network topology of the Bayesian Network can be interpreted as successional dependencies in mouse abdominal cavities. The abundance of an organism represented by a target node is dependent upon the abundance of organisms represented by its source nodes. In-degree is the number of source nodes for a target node and out-degree is the number of target nodes for a source node. A single node can be both a source node and a target node. Similar methods were used for **fig. S12.**

Soil chemistry

Five (5) replicate samples at each time point were tested for normality (Shapiro-Wilk test, R Development Core Team) and homoscedasticity (Cochran test, R). One-way analysis of variance (ANOVA, R) was used to determine if means were different between control soils and gravesoils at each timepoint (**Fig. 4A, table S13**). We also tested whether gravesoils resampled at 10, 20, and 30 days after cadaver removal (at time points day 4 and day 30) were different from control soils and the original sampling day (4 or 30) (**table S17)**. All soil chemistry data are reported in **table S18**.

PICRUSt PCoA and CCA plots

PICRUSt approach (*11*) was used to evaluate the functional potential of microbial communities. KEGG has been organized into 4 levels of hierarchies. The level one is the most general categories and the level four is the most specific - each KO terms. The analyses based on PICRUSt prediction was done on the level 3 after grouping predicted KOs into a higher level of categorization. Pairwise distances between samples were calculated using the Bray-Curtis metric on level 3 gene ontologies. We report Nearest Sequenced Taxon Index (NSTI) scores in **table S19**. The level 3 PICRUST output was also filtered to include only metabolism related gene ontologies and a second set of principal coordinates were calculated. For mouse soil samples, this metabolism-only distance matrix was used for canonical correspondence analysis, wherein sample ordinations were constrained by environmental measurements found to be significant by

an ANOVA with 1000 permutations. We plotted predicted enzyme-level gene abundances for **Figs. 3D**, **4C and fig. S13** in R using ggplot.

Gravesoils meta-analysis

We combined our soil 16S rRNA data sets with previously published swine gravesoil datasets (*26, 27*), which also followed EMP protocols. We combined these decomposition data sets with 52 soil samples from around the world (*28, 29*). We tested whether soil samples not associated with decomposition could be identified using supervised learning and report these results in the Supplementary Text.

Supplementary Text

Microbial communities in tissues and soils become more similar to each during decomposition

We discovered that microbial communities associated with cadaver tissues and surrounding soils become more similar to each other during decomposition (**fig. S15A,B)** and gravesoils become highly differentiated from control soils (**fig. S15C**). Few skin bacterial decomposer OTUs, which we defined as bacteria that differentially increased during decomposition using DESeq2, are shared across multiple experiments (**fig. S15D**). This suggests that the similarity detected using UniFrac-based metrics of bacterial decomposer communities may at higher taxonomic levels than the OTU level. Alternatively, the DESeq2 method may not capture all OTUs important for predicting PMI.

Although soil microbial communities and soil chemistry generally follow similar trends during decomposition, we did find evidence for differences as well. For example, nitrate concentrations increased in both shortgrass and desert soils, but not in forest soils (Fig. 4A). Due to the different balances between plant production and plant decomposition, as well as plant chemistry, it's common to see forest soils maintain greater organic matter concentrations and lower pH relative to more arid systems. Despite these differences, the shifts in microbial communities are similar enough across soils to allow for accurate predictions of PMI across seasons (**Fig. 1C**) and host species (**fig. S9**).

Mann-Whitney U tests of decomposer OTUs in day 1 samples

In each comparison, a higher number of decomposer OTUs was detected in soils than in abdominal samples (Mann Whitney U $p < 0.05$, **table S20**). We detected more decomposer OTUs in soils than on skin sites in most, but not all comparisons. This result is expected since the skin shares many OTUs with the outdoor environment.

Inter-domain Bayesian networks

In **Fig. 3A**, bacteria are more likely to be target nodes (p-value 0.0175). Eukaryotes are slightly more likely to be target nodes (p-value 0.0681 with only 2 eukaryotic nodes in network) and eukaryote Discicristata is a parent node of the eukaryote Nematoda. Fungi have no observed tendency to favor being source or target nodes. Root nodes of the network, nodes that have zero source nodes, are the bacteria Sphingomonadales,

Pseudomonadales; environmental conditions pH and ammonia, and the fungus Eurotiales. Leaf nodes in the network, nodes that have zero target nodes, are the bacteria Deferribacterales, Desulfovibrionales, Enterobacteriales, Lactobacillales, RF39, Rhizobiales, Bacteroidales, and Verrucomicrobiales, eukaryote Nematoda, and the fungus Hypocreales. The nodes with highest out degree (strongest drivers of community structure) are the fungus Eurotiales and environmental parameter nitrate. The nodes with highest in degrees (most dependent on the abundance of other organisms and parameters in community) all belong to bacteria: Bacillales, Bifidobacteriales, Discicristata, Clostridiales, Saprospirales, Sphingobacteriales, Bacteroidales, and Verrucomicrobiales. The most connected nodes, total in- and out-degree, are the bacteria Bacillales and Bifidobacteriales, eukaryote Discicristata, and the environmental parameter nitrate.

The soil community comprises more abundant groups resulting in a more complex network of interactions (**fig. S12A**). This community along with the skin community has more interactions dependent on soil type than in the abdominal cavity. Nitrogen plays a significant role in the interactions between multiple trophic levels including bacteria, fungi, and non-fungal eukaryotes. This latter group comprises multiple bacterivores, including nematodes and kinetoplastids (Discicristata). Interestingly, unlike in the abdominal cavity Sphingomonadales is primarily a root node, which may indicate that this group emerges from the soil environment. These analyses demonstrate the importance of nitrogen in community interactions, which are modulated by environment (total nitrogen is always a terminal node). The open systems are more influenced by the environment than the closed system.

PICRUSt predictions

We report our Nearest Sequenced Taxon Index (NSTI) scores for our PICRUSt analysis (**table S19**). According to the if the score is 0.03 it indicates that the average microbe in our sample can be predicted using a relative from the same (97%) species. In our case 2040/2110 are above this threshold. Therefore we believe our predictions have believable implications for metabolic function of the community.

Soil fingerprint of decomposition and its persistence after cadaver removal

We confirmed previously published findings (*7*) indicating that decomposing cadavers substantially modify soil microbial communities (**figs. S2–S4**, **fig. S16C**). Building on these results, a meta-analysis of our soil 16S rRNA data with previously published swine gravesoil data sets (*26*, *27*) and a broadly representative soil data set (*28, 29*). A Random Forests classifier allowed us to accurately distinguish the probability of a soil being associated with decomposition (>99% accuracy in all soils except desert, which was 94% accurate) (**fig. 17A**). We also showed that a subset of soil decomposers (significantly increasing OTUs) and soil taxa that decrease during decomposition (as described in methods using DESeq2) were shared across our experiments and soil types (**fig. 17B**). However, when soils data sets were combined with swine gravesoils, we did not detect any significantly increasing or decreasing OTUs shared among all datasets (**fig. 17C)**. This result indicates that decomposer microbial community similarity is likely at a higher taxonomic level than OTU.

Finally, we tested whether soil chemistry and microbial markers persisted in soils for up to 30 days after mouse cadavers were removed. We discovered that postmortem soil chemistry biomarkers (**fig. S18, table S17**) and microbial community fingerprints can persist in gravesoils for up to 30 days (**fig. S19**). Therefore, gravesoils are a promising avenue for identifying the location of clandestine graves, and whether a cadaver has been moved.

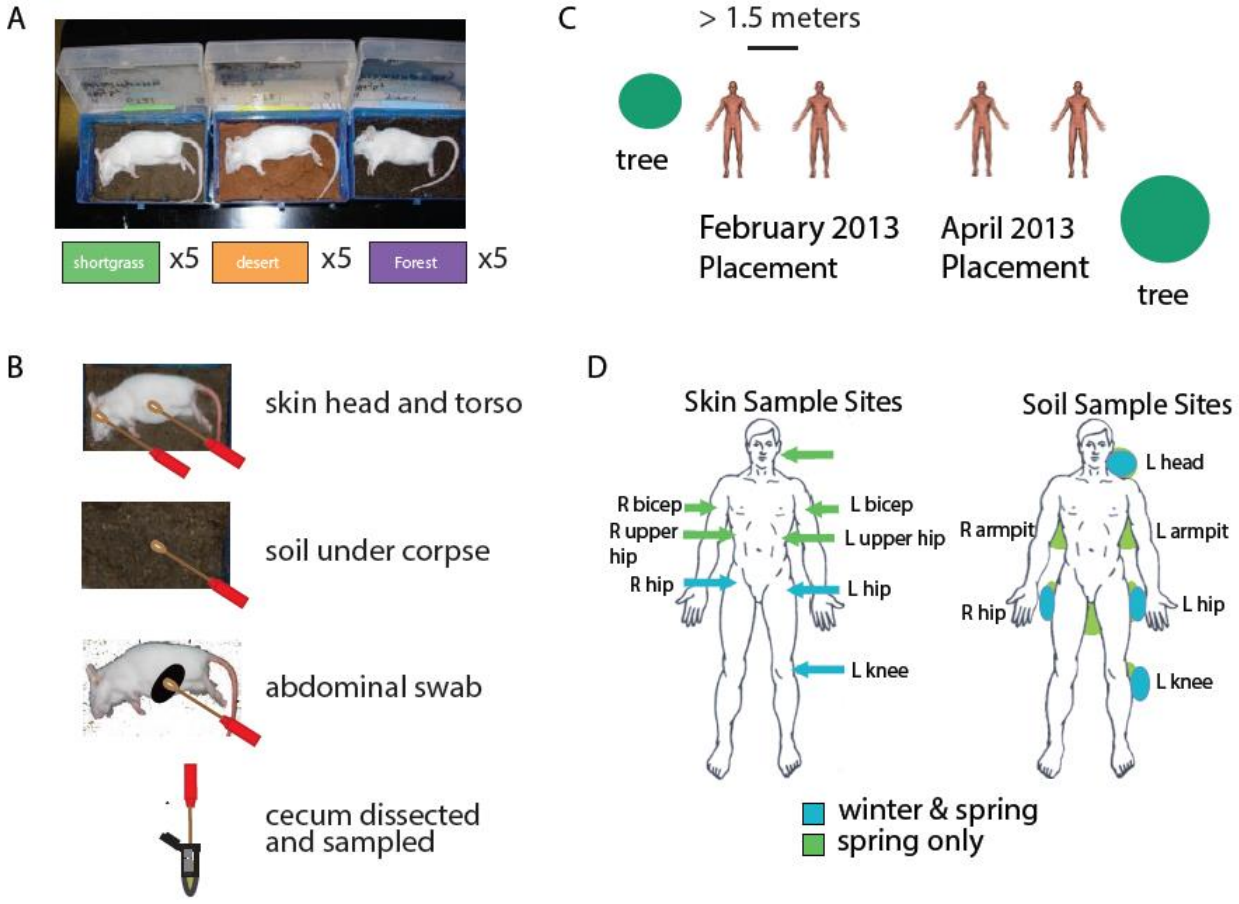

Fig. S1

Experimental setup for mice on three contrasting soil types, and human subjects at STAFS facility over two seasons. (A) We destructively sampled five mice per time point per soil type (shortgrass prairie, desert, forest) for eight time points, along with five control soils of each soil type for each time point. (B) For each mouse, we sampled the skin of the head and torso, the soil under the corpse, and abdominal cavity and cecum via dissection. For two sample time points (days 3 and 29), we also resampled the soil from each grave 10, 20, and 30 days after the mouse cadaver was removed. (C) Two human subjects were placed in winter and spring seasons at the STAFS. (D) Multiple skin and soil locations were sampled throughout the experiment.

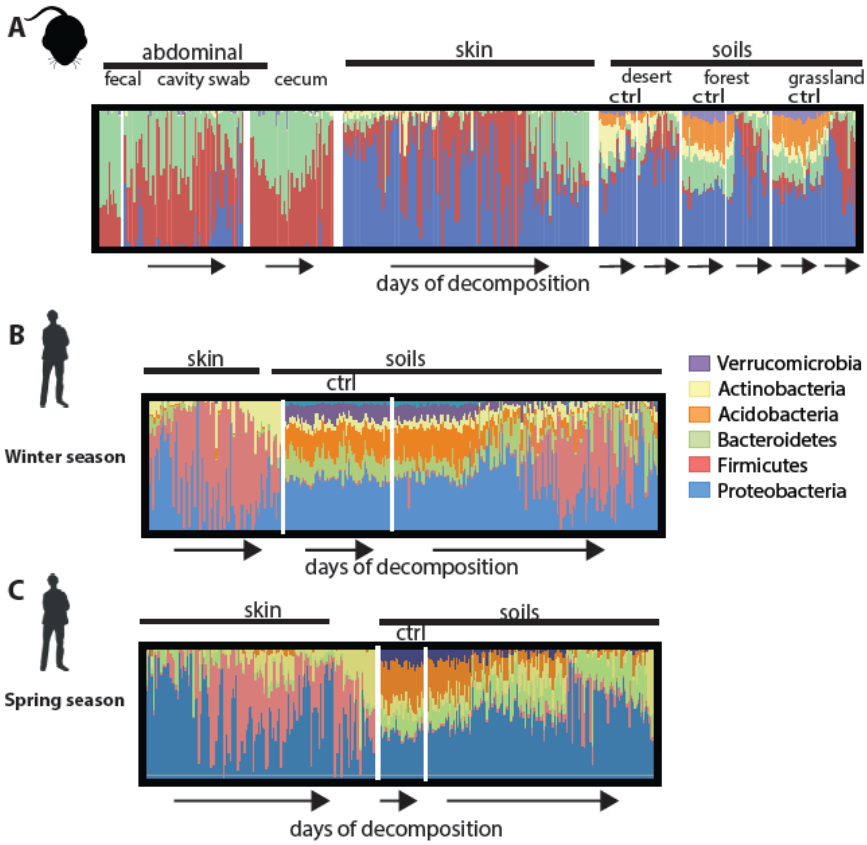

Fig. S2

Relative abundance of bacterial phyla characterized by 16S rRNA amplicon sequencing in **(A)** laboratory mouse experiment, **(B)** human experiment (winter season), and **(C)** human experiment (spring season). Samples are grouped by sample type and ordered by time of decomposition (days since placement). Each bar represents the relative abundance of the bacterial community of a single sample. Phyla that were represented by <0.1% of the total data set are not shown in plot.

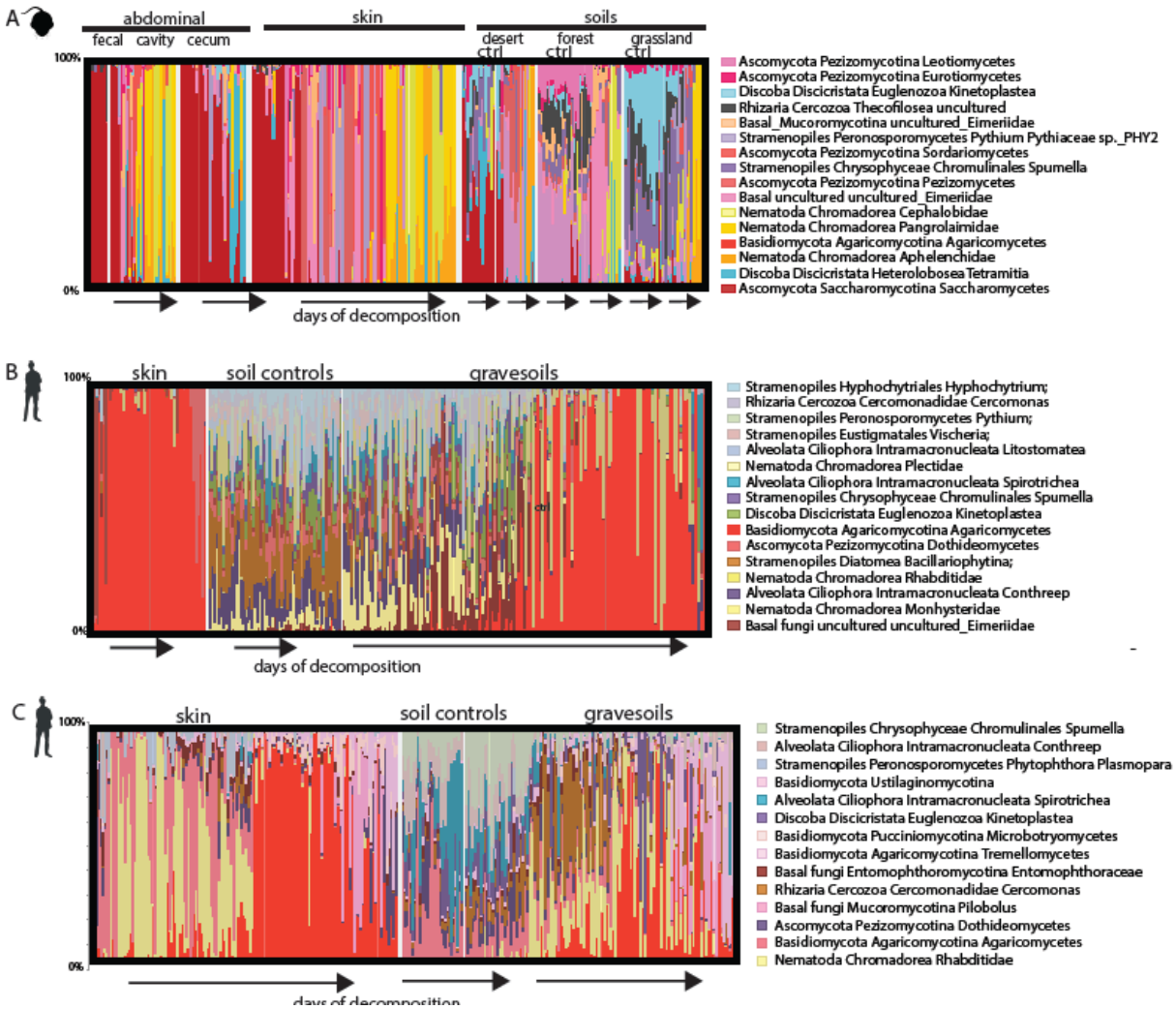

Fig. S3

Relative abundance of microbial eukaryotes characterized by 18S rRNA amplicon data for the laboratory mouse experiment. Each bar represents the relative abundance of the bacterial community of a single sample. (A) In the mouse model experiment, all sample sites except for the cecum, which was only sampled through day 14 or 29 depending on visible access to the cecum, nematodes (Class Chromadorea) become highly abundant**.** **(B)** Relative abundance of microbial eukaryotic taxa during decomposition in skin, soil controls, and gravesoils for the February field experiment**.** (C) Relative abundance of microbial eukaryotic taxa during decomposition in skin, soil controls, and gravesoils for the February field experiment. Fungal taxa are represented by shades of red or pink and nematodes are represented with shades of yellow or orange. In skin and soil samples, an increase in nematode relative abundance (yellow) is evident, particularly in the mouse experiment and the human spring experiment. Taxa represented by <0.1% of the total data set are not shown in plot.

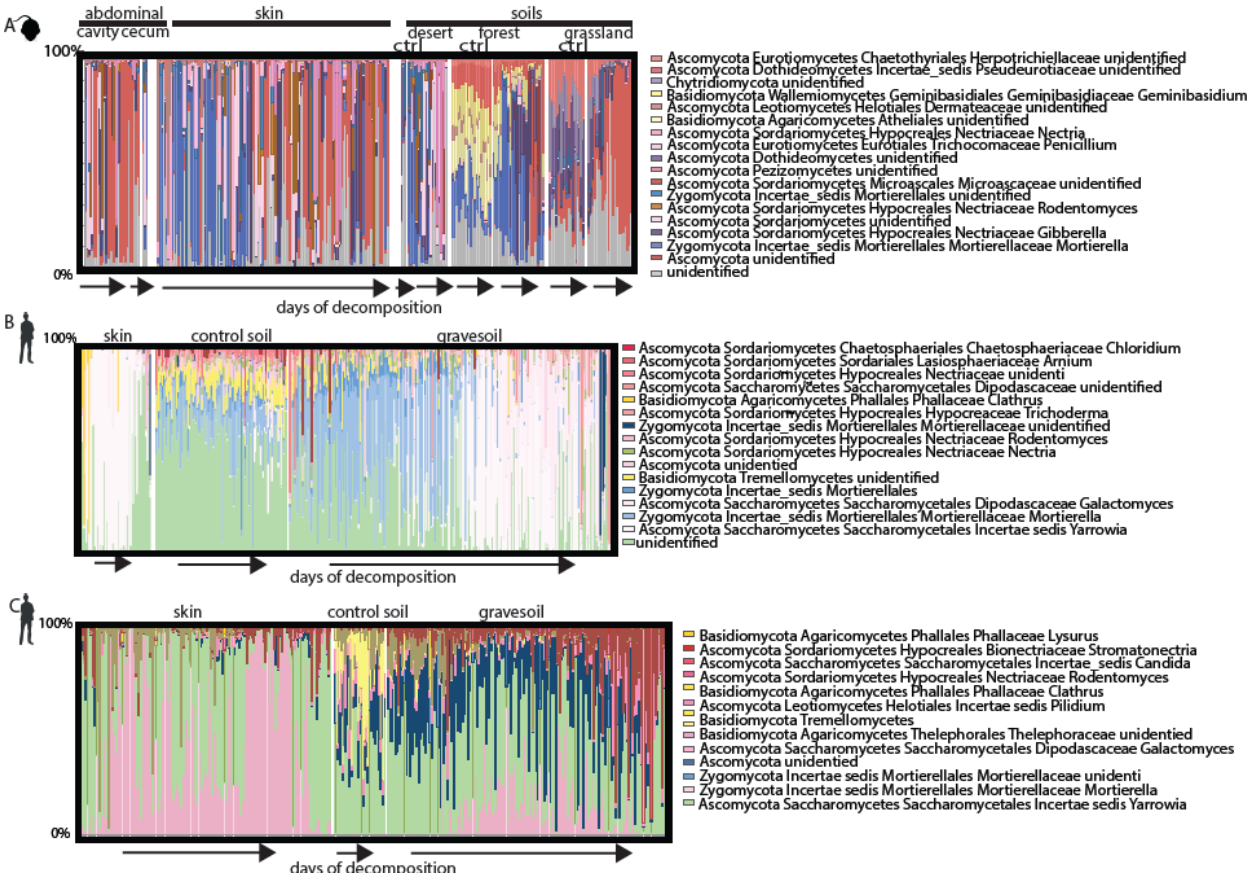

Fig. S4

Relative abundance of fungal taxa during decomposition. Each bar represents the relative abundance of the bacterial community of a single sample. **(A)** mouse model experiment, **(B)** human model winter experiment, and **(C)** human model spring experiment. Taxa in the group Ascomycota are shaded red/pink, Basidiomycota are shaded yellow, and Zygomycota are shaded blue. Fungi represented by <0.1% of the total data set are not shown in plot.

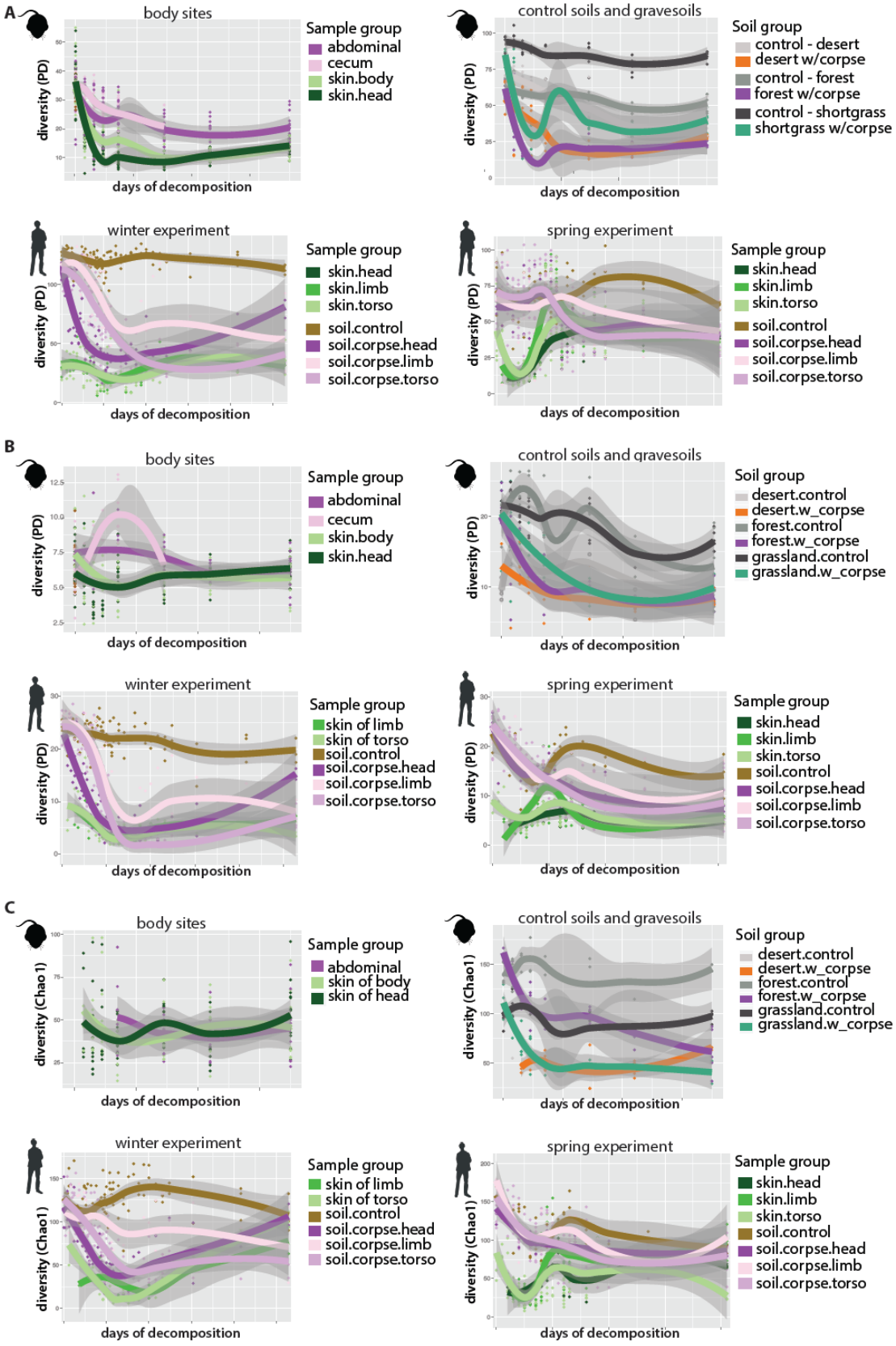
A
body sites
diversity (PD)
days of decomposition
Sample group
abdominal
cecum
skin.body
skin.head
control soils and gravesoils
Soil group
control - desert
desert w/corpse
control - forest
forest w/corpse
control - shortgrass
shortgrass w/corpse
winter experiment
skin.limb
skin.torso
soil.control
soil.corpse.head
soil.corpse.limb
soil.corpse.torso
spring experiment
B
desert.control
desert.w_corpse
forest.control
forest.w_corpse
grassland.control
grassland.w_corpse
skin of limb
skin of torso
C
diversity (Chao 1)
skin of body
skin of head

Fig. S5
Alpha diversity (PD) of the microbial communities. (A) Relative abundance of bacterial phyla characterized by 16S rRNA amplicon sequencing in laboratory mouse experiment (upper) field experiment with human subjects (lower). Samples are grouped by sample type and ordered by time of decomposition (days since placement). (B) phylogenetic diversity estimate based on 18S rRNA data. (C) Chao1 diversity estimate based on ITS. For most samples, alpha diversity decreases during decomposition in microbial communities, especially in gravesoils compared to controls soils. In the mouse model experiment, we detected an increase followed by a decrease in diversity of the cecum and abdominal cavity. We also detected variation in the alpha diversity of the control soils.

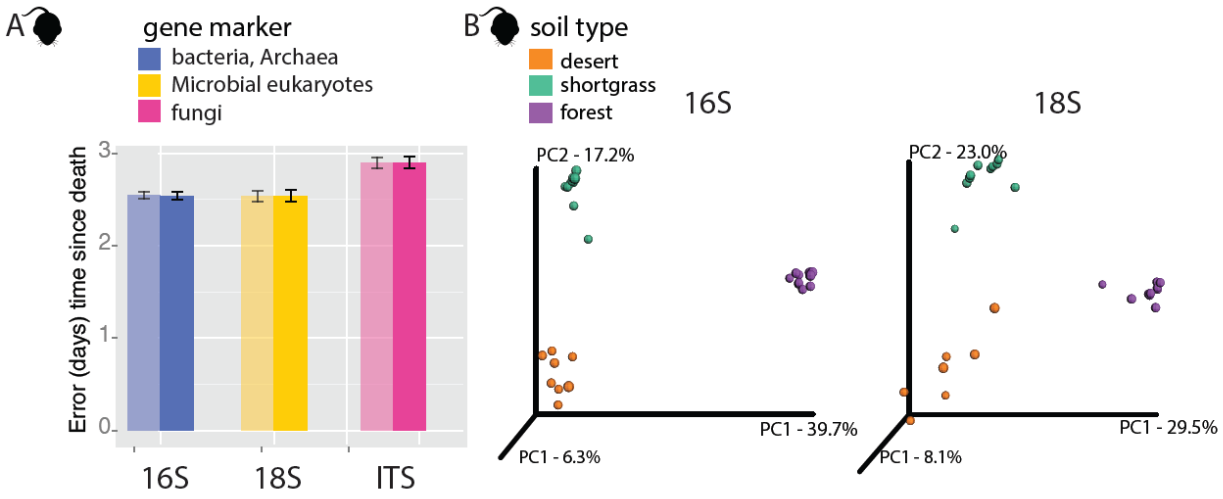

Fig. S6

Differences in starting soil microbial communities do not affect regression accuracy. (A) RMSE estimates for the first 14 days of mouse model experiment with soil type included (dark bars) and not included (light) as a feature in the regression models for each marker type (16S, 18S, ITS). Importantly, accuracy was not improved by including soil type as a feature in our regression models. (B) PCoA plots based on UniFrac distance of bacterial (left) and microbial eukaryotic (right) soil communities at the start of the experiment. Each soil type hosted a microbial community with distinct community structure.

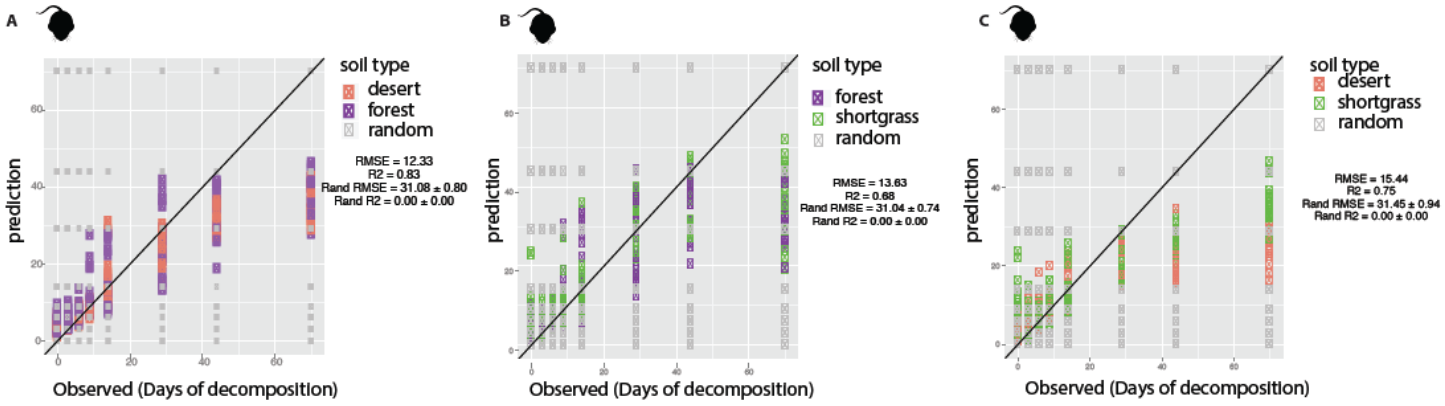

Fig. S7
A random forest (RF) model built from 16S rRNA skin, abdominal and soil data from mice decomposing on (A) shortgrass prairie soil (B) desert soil and (C) forest soil, and used to estimate PMI accuracy for mice decomposing on (A) desert and forest soils (B) forest and grassland soils and (C) desert and grassland soils. RF predicted PMI in orange and green (see legends), and random predictions in gray.

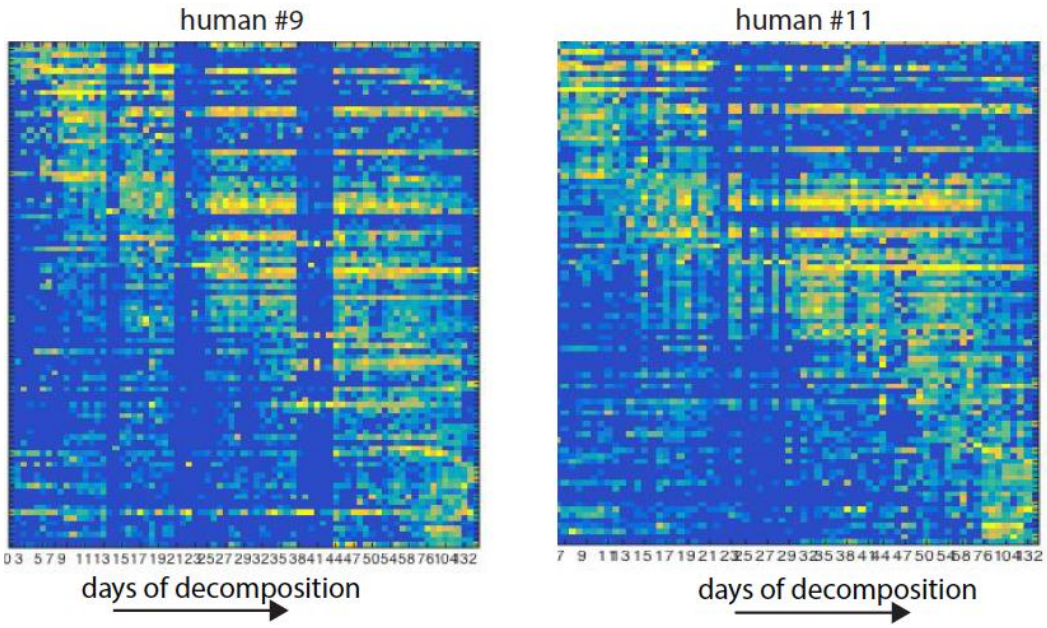

Fig. S8
A heat map (blue = low abundance, yellow = high abundance) of bacteria colonizing the human subjects (#9 left and #11 right) in the winter season experiment sorted according to colonization time of Human #9. Generally, the same bacteria colonized bodies at approximately the same time within an experiment.

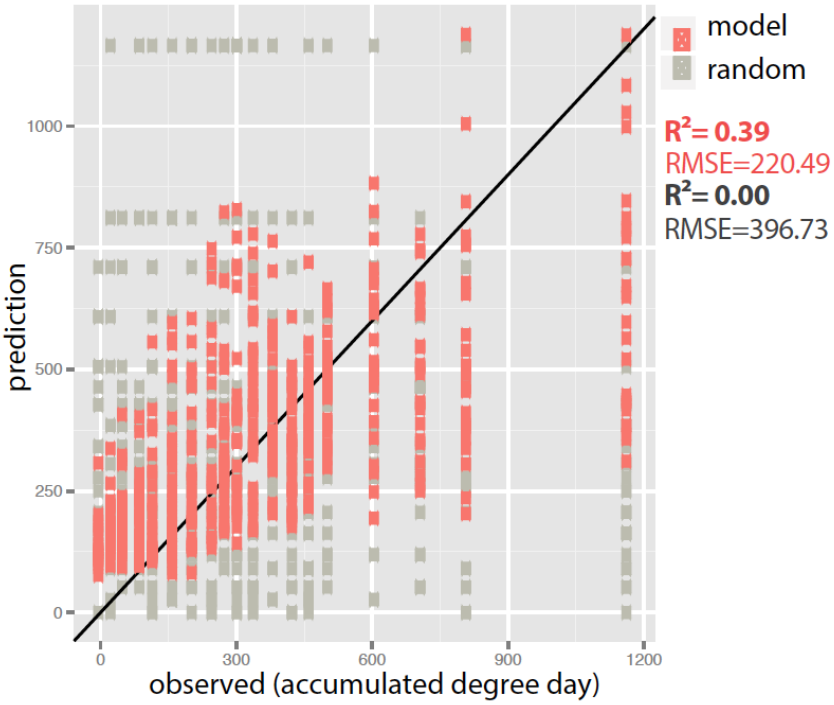

Fig. S9
A 16S rRNA-based Random Forests (RF) model using mouse decomposition data to train the model and predict the PMI of human body. Each point in the plot indicates a sample collected at a certain PMI, with RF predicted PMI in red and randomly guessed PMI in gray.

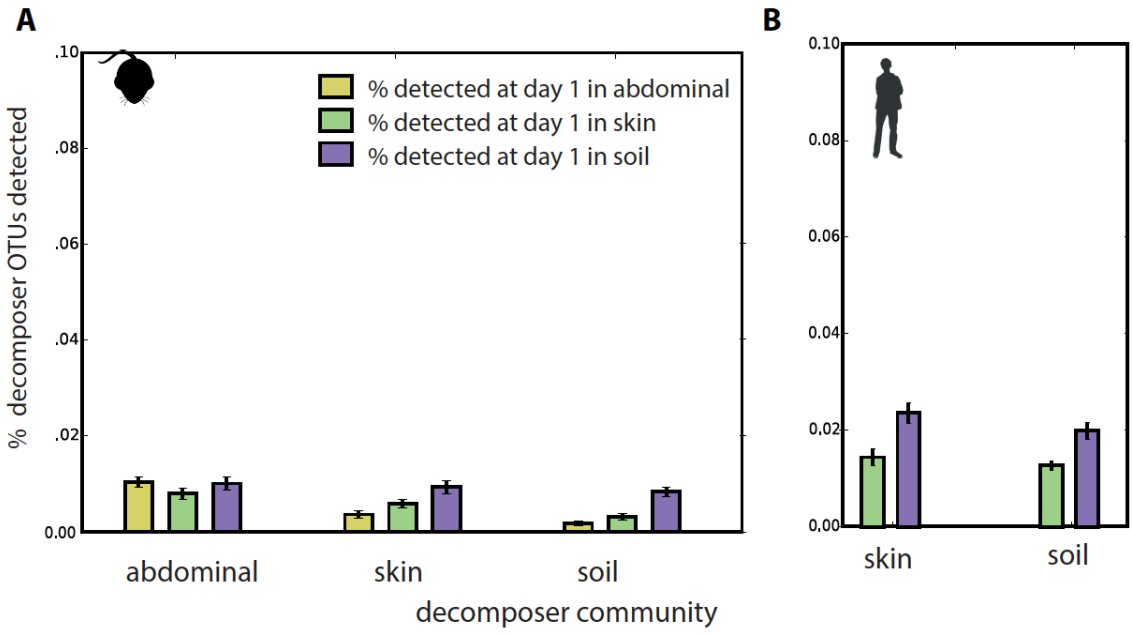

Fig. S10

Proportion of decomposer bacteria discovered in fly samples (not deeply sequenced as in Fig 2B) in mice cadavers (A) and human cadavers (B). In the mouse experiment bars are ordered by soil type (desert, shortgrass, forest). In the human experiments, bars are ordered by season (winter, spring). Bars are shown with standard error. In most cases <2% of insect taxa were detected in day 1 communities.

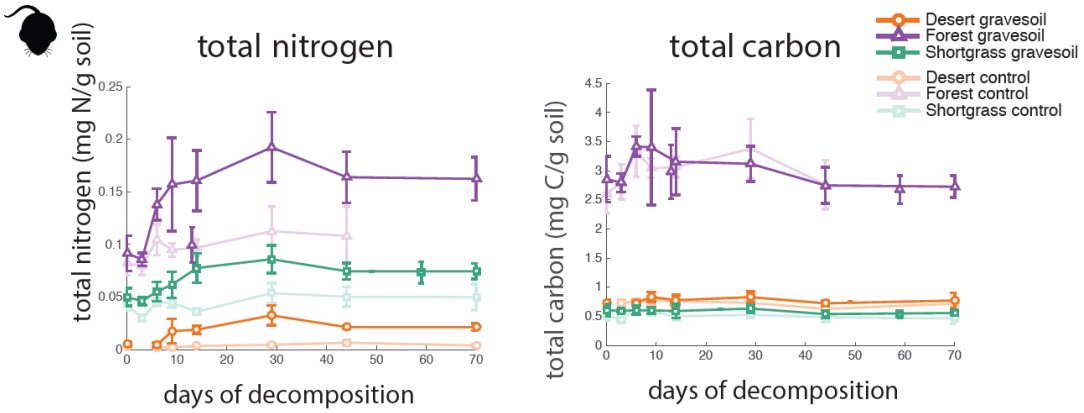

Fig. S11
Levels of total nitrogen and total carbon in mouse gravesoils compared to control soils during decomposition.

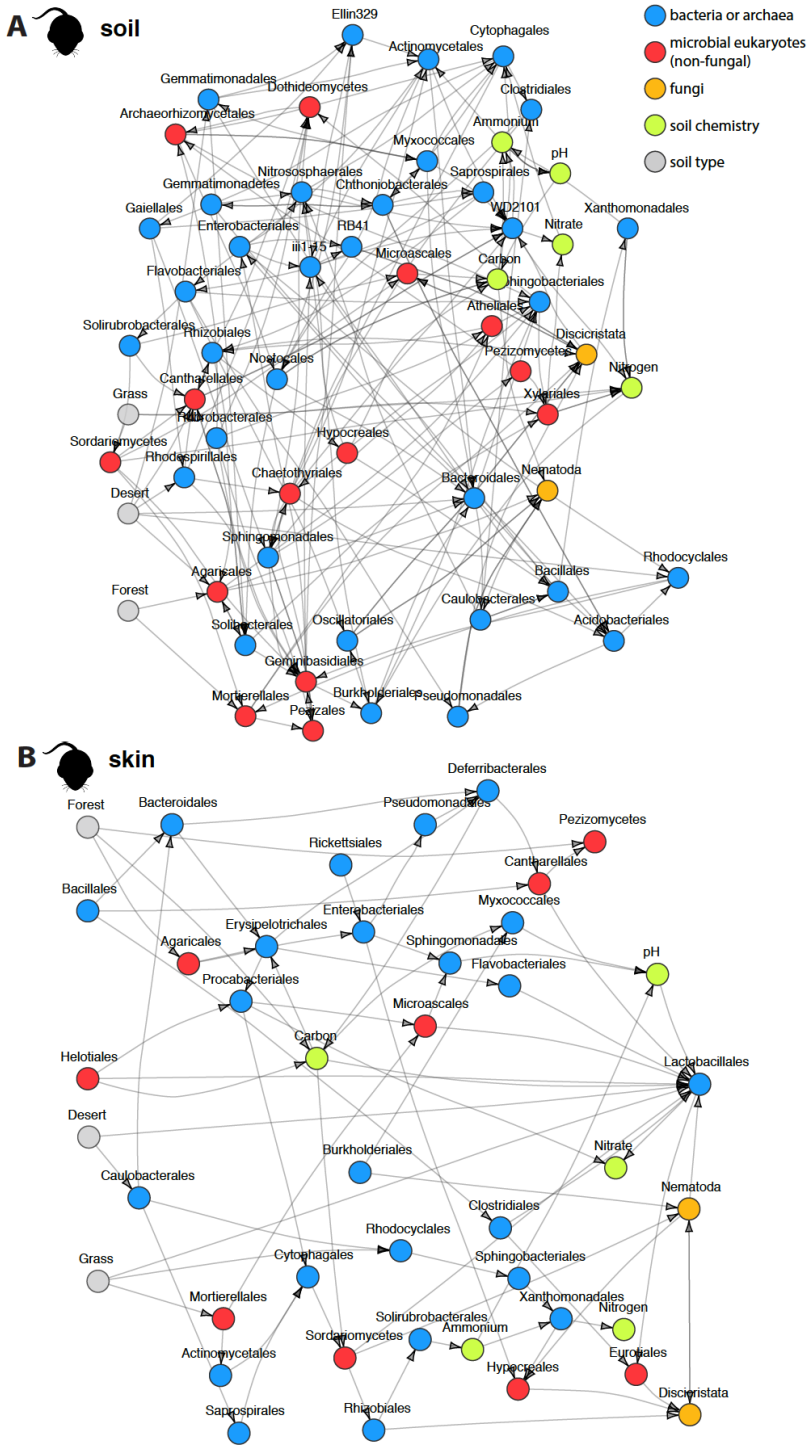

Fig. S12

Dynamic Bayesian Networks of interactions between members of the decomposer community. Arrows indicate direction of causality between changes in the abundance of bacterial classes (blue nodes), fungal classes (red nodes), non-fungal eukaryotic groups (orange), and environmental factors (green). Interactions conditional on soil type are connected to soil nodes (grey).

Fig. S13

Predicted gene abundances for all gravesoil samples with mouse experiment results shown in orange (desert), green (shortgrass), and purple (forest), and human gravesoils in blue. Pathway results are grouped by pathway category.

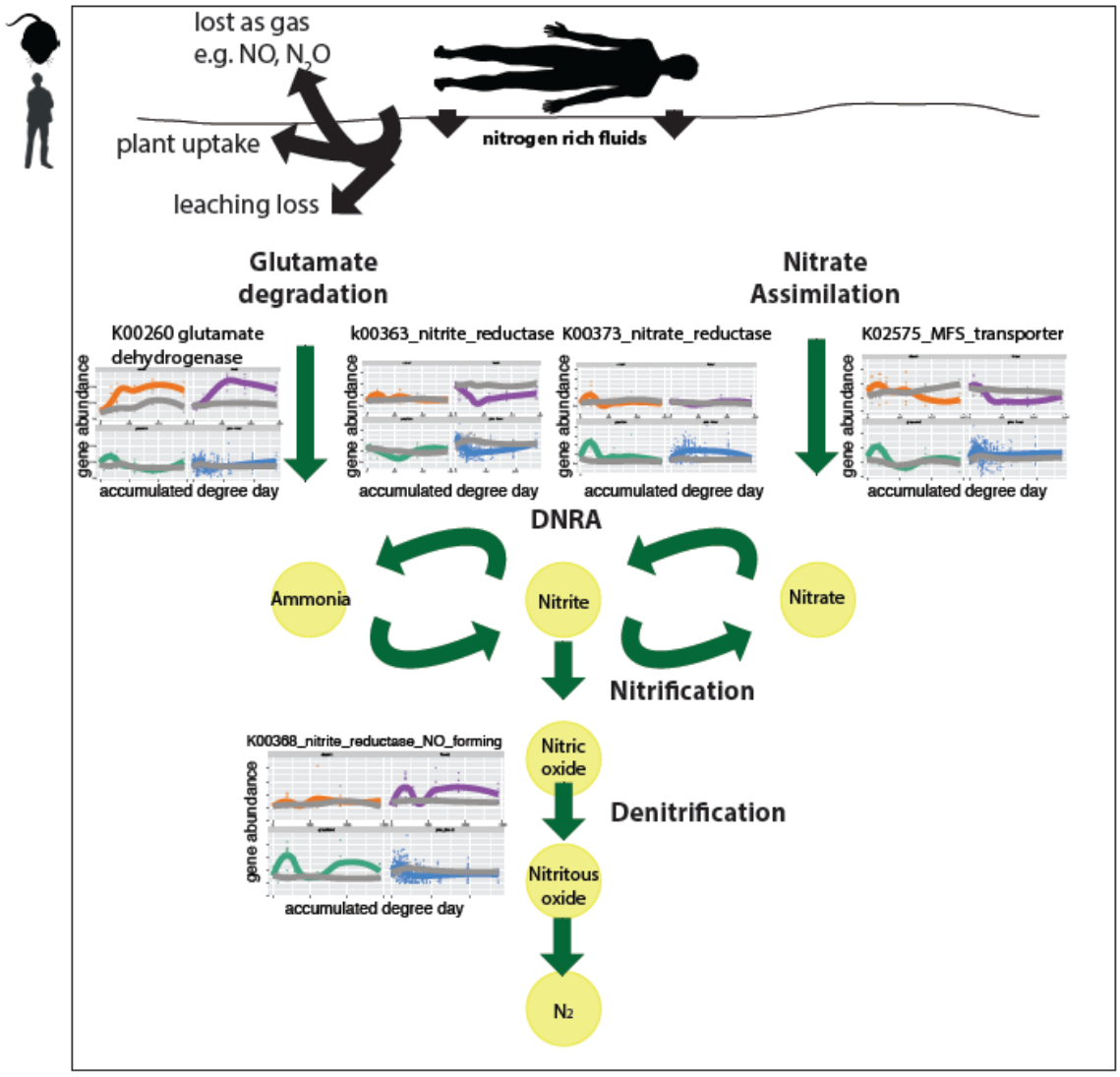

Fig. S14
Summary schematic of mammalian decomposition effects on surrounding soils with the nitrogen cycle pathways supported by functional inferences from bacteria highlighted in dark green. Cadaver-derived amino acids such as glutamate degrade and generate high concentrations of ammonia (NH_3), which bond with protons to form ammonium (NH_4^+) ions causing a spike in soil pH. Plots show predicted gene abundances during decomposition of relevant gene pathways with mouse experiment results shown in orange (desert), green (shortgrass), and purple (forest), and human gravesoils in blue. A gray line shows predicted gene abundances in control soils.

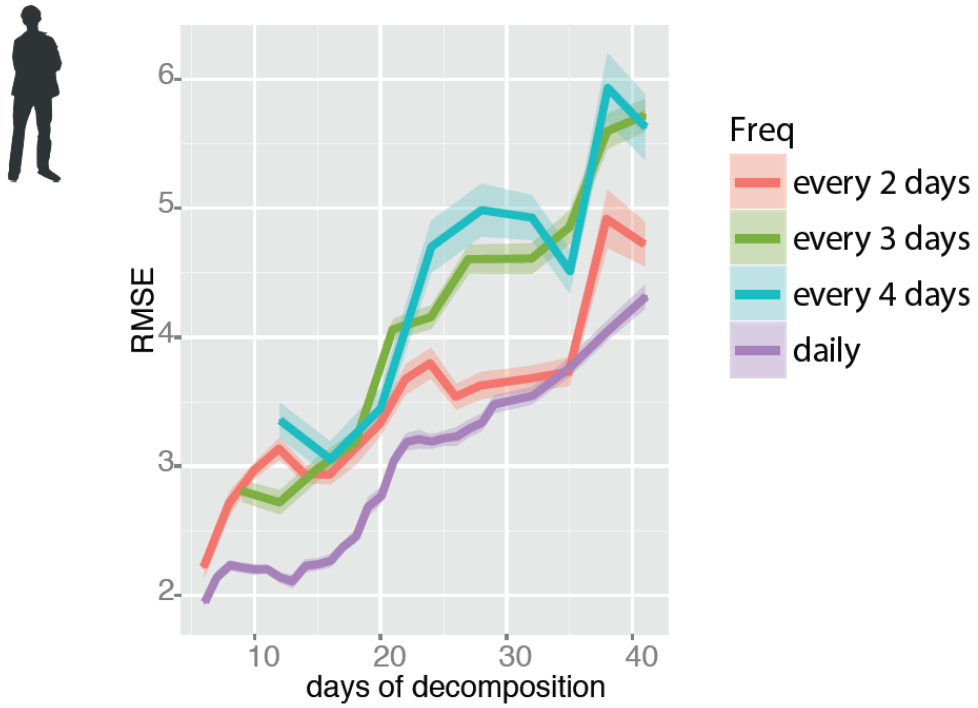

Fig. S15
Using 16S rRNA data from the daily-sampled SHSU winter experiment, we subsampled the data at different sampling frequencies. Daily sampling provided the most accurate estimates of PMI.

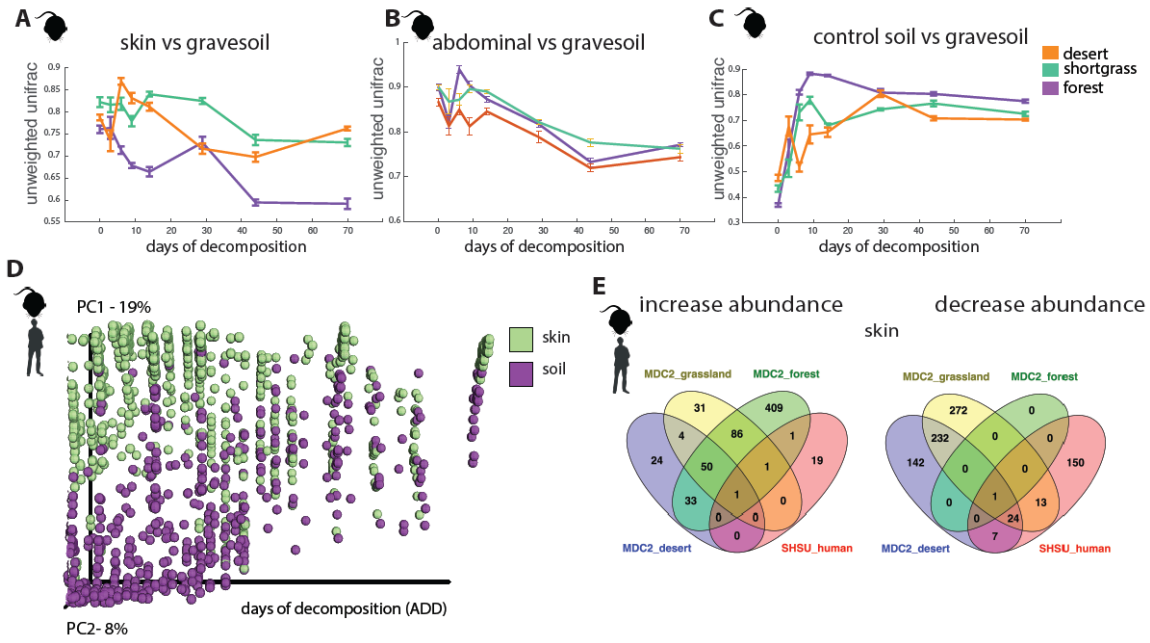

Fig. S16

Mean unweighted UniFrac distance between sample types during decomposition of (A) skin vs. gravesoil (B) abdominal vs. gravesoil and (C) control soil samples vs. gravesoil. Purple, orange, and green lines represent the mean distances for forest, grassland and desert soils respectively, and error bars represent the standard error for the distances.(D) PCoA plot based on unweighted UniFrac distance of skin and soil samples in all experiments during decomposition showing that all skin samples increasingly cluster with soils as decomposition progresses. Of the skin bacterial taxa that differentially increased (left) or decreased (right) in abundance during decomposition, some were common across multiple experiments as illustrated with the Venn diagram.

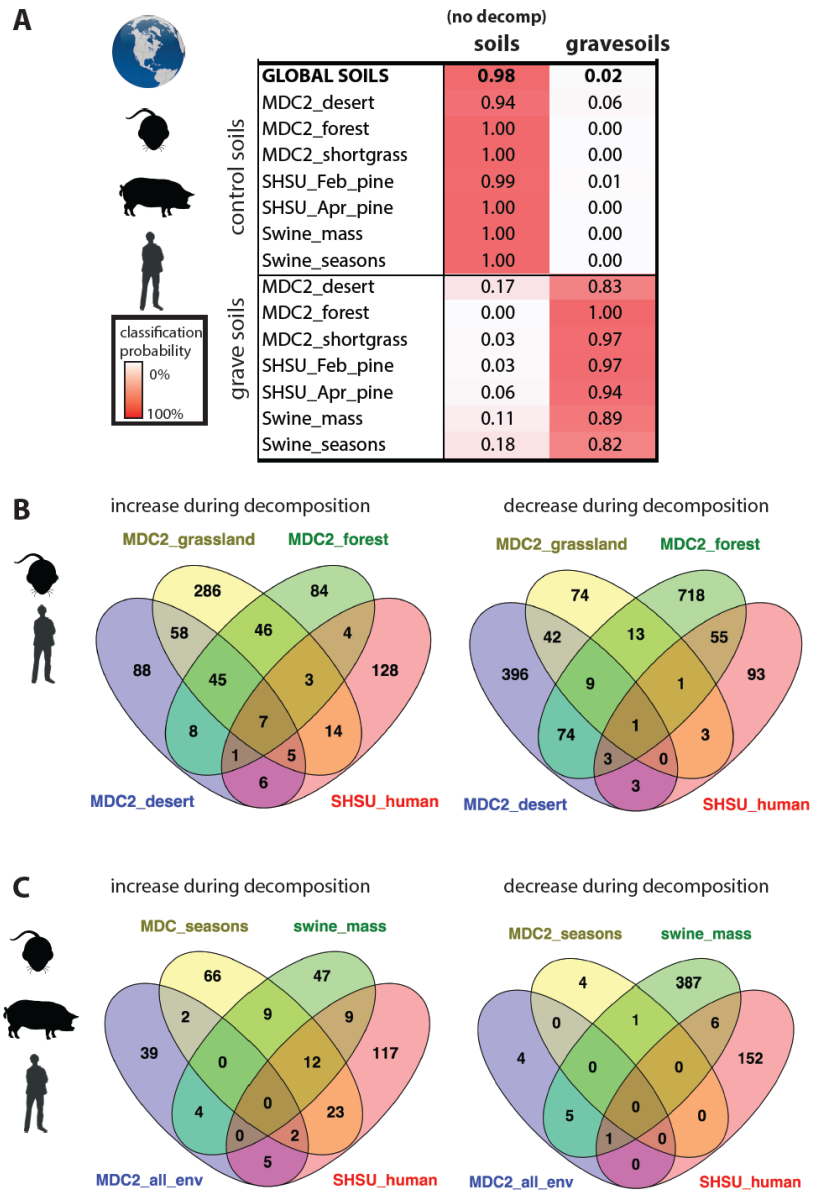

Fig. S17

Decomposition significantly modifies soil microbial communities. (A) experimental control and gravesoils were combined with a global soils data set. A Random Forests classifier allowed us to accurately distinguish the probability of a soil being associated with decomposition (>99% accuracy in all soils except desert, which was 94% accurate). (B) Of the soil bacterial and archaeal taxa that differentially increased (left) or decreased (right) abundance during decomposition in mouse and human data sets, some were shared across experiments and soil types as illustrated with the Venn diagram. (C) When soils data sets were combined with similarly generated swine gravesoils, we did not detect any significantly increasing or decreasing OTUs shared among all datasets.

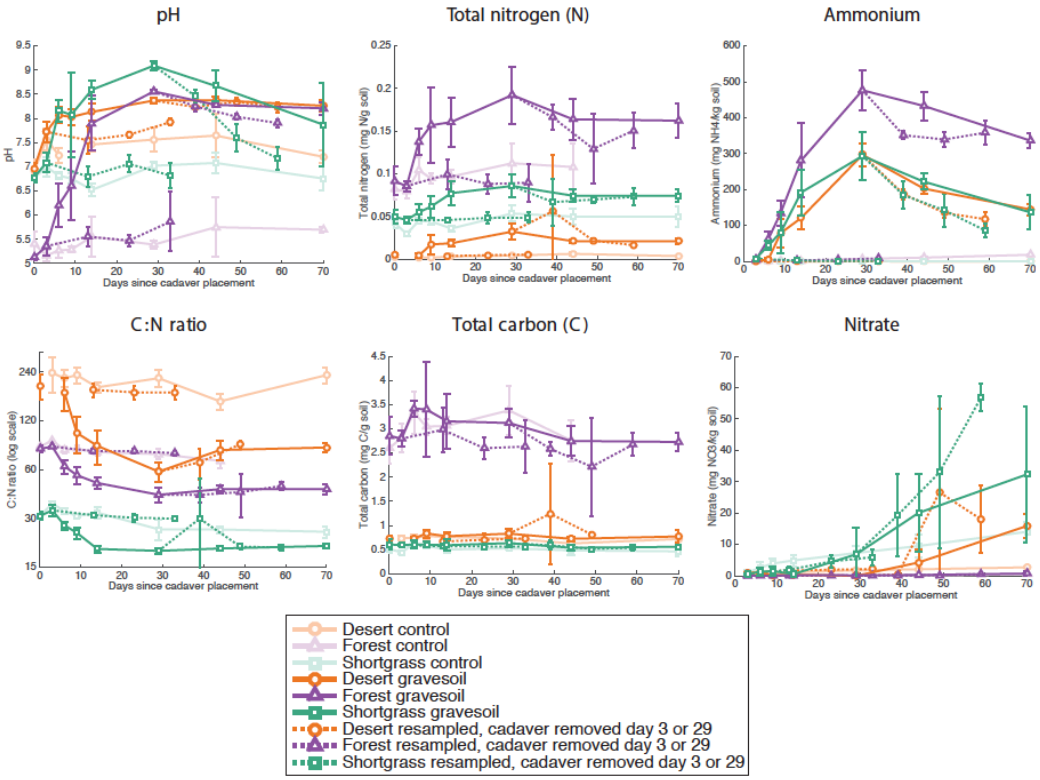

Fig. S18
Soil chemistry dynamics during decomposition. Solid lines represent gravesoil chemistry after cadaver replacement, with lighter colors indicating control soils. Dotted lines represent gravesoils resampled 10, 20, and 30 days after cadaver removal (at timepoints day 3 and day 29). ANOVA results can be found in table S1.

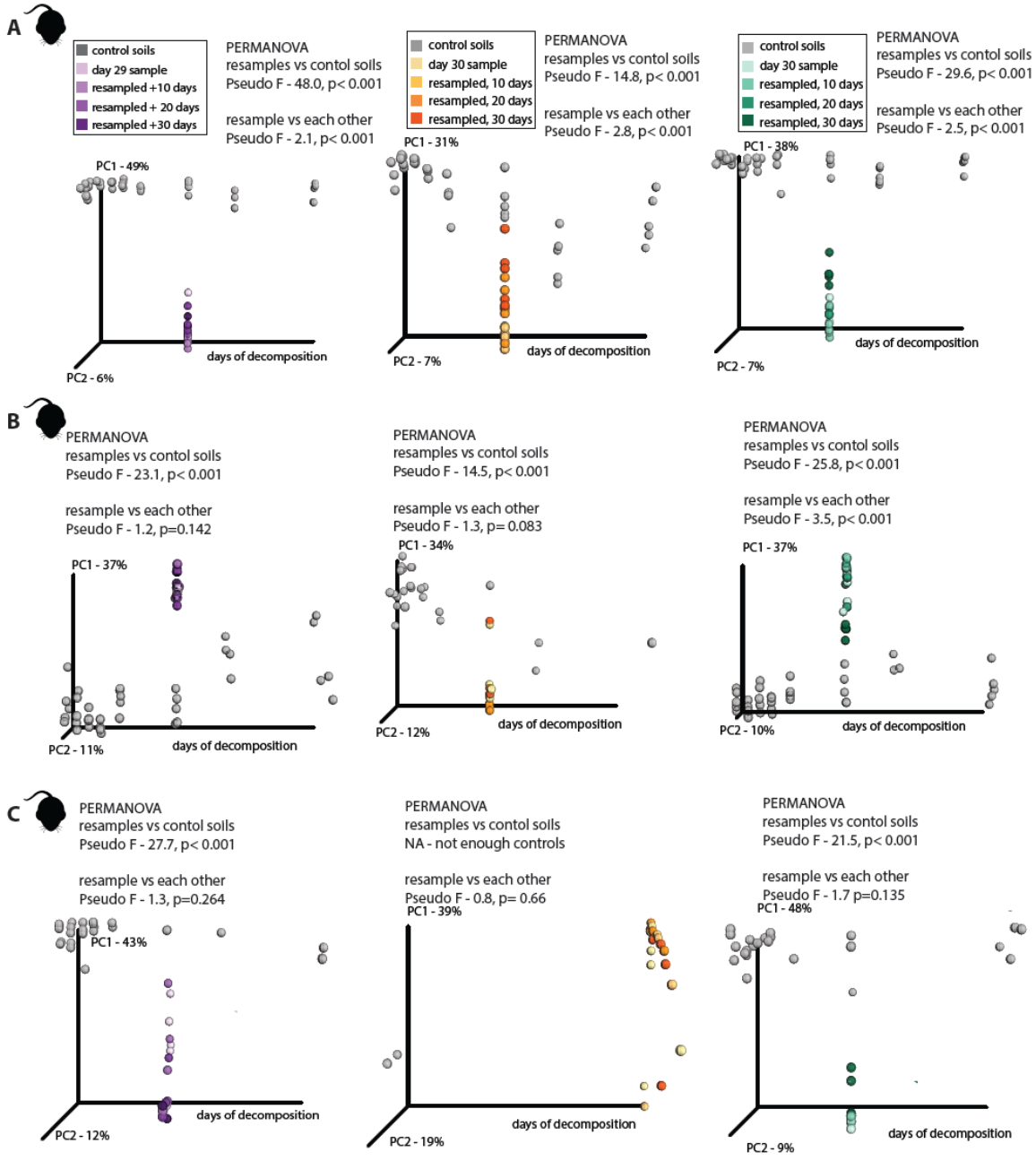

Fig. S19

Gravesoil microbial decomposer communities persist for at least 30 days after a cadaver is removed. (A) Forest (purple), desert (orange), and shortgrass prairie (green) gravesoils were sampled after 30 days (post-rupture) of mouse cadaver decomposition, and resampled 10, 20, and 30 days after the cadaver was removed. (A) 16S rRNA data (B) 18S rRNA data (C) ITS gene data set. Gravesoils (color) are compared to control soils (gray), illustrating that the bacterial decomposer community persists in the gravesoil for at least 30 days under laboratory conditions.

Table S1.

Results of ANOSIM and PERMANOVA tests on unweighted UniFrac distance matrix generated from mouse-model experiment 16S rRNA amplicon data set. All comparisons of decomposition-associated of archaeal and bacterial communities were significantly different from their starting community. Additionally, the three contrasting control soil types were significantly different from each other, and were still significantly different from each other during decomposition, but less so (lower R-value and Pseudo-F value).

Comparison	ANOSIM R	ANOSIM p-value	PERMANOVA Pseudo-F	PERMANOVA p-value
Soil controls vs. soil with corpse	0.3814	0.001	27.9644	0.001
Soil controls vs. post-rupture gravesoil	0.6665	0.001	40.8150	0.001
soil controls by soil type	0.9280	0.001	50.3424	0.001
soils with corpse by soil type	0.4289	0.001	10.4011	0.001
soils with corpse advanced decay by soil type (no control soils)	0.6745	0.001	11.0273	0.001
Skin day 0 vs. skin advanced decay	0.6984	0.001	26.5322	0.001
Skin advanced decay by sample location	0.0808	0.001	3.3125	0.001
Abdomen day 0 vs. abdomen advanced decay	0.2333	0.002	7.4745	0.001
Cecum day 0 vs. cecum advanced decay	0.1727	0.022	8.5032	0.001

Table S2.

Results of nonparametric t-tests on levels of phylogenetic diversity between groups from mouse-model experiment 16S rRNA amplicon data set. All comparisons of decomposition-associated archaeal and bacterial communities were significantly different from their starting community. P-values have been Bonferroni corrected for multiple comparisons.

Laboratory experiment, 16S							
Group1	Group2	G1 mean	G1 sd	G2 mean	G2 sd	t-stat	p
Soil controls	soil with corpse	66.726	18.719	42.167	22.645	9.857	0.015
Soil controls	soil with corpse advanced decay	66.726	18.719	29.508	13.017	-18.244	0.015
desert soil control	forest soil control	55.479	16.953	56.044	6.706	-0.192	12.885
desert soil control	grassland soil control	55.479	16.953	87.248	8.065	10.422	0.015
forest soil control	grassland soil control	56.044	6.706	87.248	8.065	18.578	0.015
desert soil with corpse	forest soil with corpse	40.688	19.352	32.234	18.412	2.600	0.165
desert soil with corpse	grassland soil with corpse	40.688	19.352	53.602	24.397	3.410	0.045
forest soil with corpse	grassland soil with corpse	32.234	18.412	53.602	24.397	5.722	0.015
desert soil advanced decay	forest soil advanced decay	30.649	13.298	19.808	5.252	4.972	0.015
desert soil advanced decay	grassland soil advanced decay	30.649	13.298	38.066	11.633	-2.753	0.120
forest soil advanced decay	grassland soil advanced decay	19.808	5.252	38.066	11.633	9.380	0.015
skin day 0	skin advanced decay	37.404	8.268	13.019	4.997	21.797	0.015
skin (body) advanced decay	skin (head) advanced decay	11.503	3.364	14.570	5.847	-4.154	0.015
abdomen day 0	abdomen advanced decay	33.118	8.302	21.335	7.213	-5.618	0.015
cecum day 0	cecum advanced decay	34.661	3.605	26.871	5.020	-5.479	0.015

Table S3.

Results of ANOSIM and PERMANOVA tests on unweighted UniFrac distance matrix generated from 16S rRNA amplicon data sets of human-model field experiments. All comparisons of decomposition-associated of archaeal and bacterial communities were significantly different from their starting community.

Field experiment February, 16S				
Comparison	ANOSIM R	ANOSIM p-value	PERMANOVA Pseudo-F	PERMANOVA p-value
Soil controls vs. soil with corpse	0.0590	0.024	54.8817	0.001
Soil controls vs. soil with corpse advanced decay	0.4992	0.001	49.7761	0.001
Skin day 0 vs. skin advanced decay	0.6080	0.001	3.0763	0.001
Soil advanced decay by sample location	0.1957	0.001	3.9064	0.001
Skin advanced decay by sample location	0.0215	0.076	1.7773	0.132
Field experiment April, 16S				
Comparison	ANOSIM R	ANOSIM p-value	PERMANOVA Pseudo-F	PERMANOVA p-value
Soil controls vs. soil with corpse	0.0026	0.446	19.5608	0.001
Soil controls vs. soil with corpse advanced decay	0.4057	0.001	21.8429	0.001
Skin day 0 vs. skin advanced decay	0.3436	0.001	2.9788	0.004
Soil advanced decay by sample location	0.1058	0.001	3.1571	0.001
Skin advanced decay by sample location	0.0478	0.001	1.7593	0.001

Table S4.

Results of nonparametric t-tests on levels of phylogenetic diversity between groups from 16S rRNA amplicon data sets of human-model field experiments. Comparisons of diversity in decomposition-associated of archaeal and bacterial communities of soil, but not skin, were significantly different from their starting community. P-values have been Bonferroni corrected for multiple comparisons.

Field experiment Feb, 16S							
Group1	Group2	G1 mean	G1 sd	G2 mean	G2 sd	t-stat	p
soil controls	soil with corpse	121.387	7.714	77.445	33.241	14.174	0.007
soil controls	soil with corpse advanced decay	121.387	7.714	53.581	23.956	29.255	0.007
skin day 0	skin advanced decay	24.778	4.344	25.609	11.518	-0.142	6.216
soil head	soil limb	44.370	15.812	72.416	31.022	-4.469	0.007
soil head	soil torso	44.370	15.812	50.245	19.232	-1.505	0.945
soil limb	soil torso	72.416	19.232	50.245	19.232	-4.177	0.007
skin head	skin limb	NA	NA	27.059	12.025	NA	NA
skin head	skin torso	NA	NA	24.932	11.210	NA	NA
skin limb	skin torso	27.059	12.025	24.932	11.210	0.801	2.961
Field experiment April, 16S							
soil controls	soil with corpse	68.529	15.472	58.743	20.718	3.254	0.018
soil controls	soil with corpse advanced decay	68.529	15.472	57.027	20.563	3.819	0.009
skin day 0	skin advanced decay	43.901	21.935	37.338	22.692	0.638	4.869
soil head	soil limb	55.578	17.610	60.501	20.145	-1.041	2.718
soil head	soil torso	55.578	17.610	56.625	21.110	-0.266	7.173
soil limb	soil torso	60.501	20.145	56.625	21.110	-0.966	3.033
skin head	skin limb	31.164	17.385	41.916	24.611	-2.216	0.342
skin head	skin torso	31.164	17.385	35.863	21.964	-1.105	2.313
skin limb	skin torso	41.916	24.611	35.863	21.964	1.871	0.558

Table S5.

Results of ANOSIM and PERMANOVA tests on unweighted UniFrac distance matrix generated from 18S rRNA amplicon data sets of mouse-model field experiments. All comparisons of decomposition-associated of microbial eukaryotic communities were significantly different from their starting community with the exception of the abdominal cavity.

Laboratory experiment, 18S				
Comparison	ANOSIM R	ANOSIM p-value	PERMANOVA Pseudo-F	PERMANOVA p-value
Soil controls vs. soil with corpse	0.2846	0.001	20.0520	0.001
Soil controls vs. soil with corpse advanced decay	0.4654	0.001	30.0921	0.001
soil controls by soil type	0.7681	0.001	24.7448	0.001
soils with corpse by soil type	0.3107	0.001	8.4948	0.001
soils with corpse advanced decay by soil type (no control soils)	0.3903	0.001	15.3734	0.001
Skin day 0 vs. skin advanced decay	0.4022	0.001	21.6748	0.001
Skin advanced decay by sample location	0.0134	0.094	1.8097	0.094
Abdomen day 0 vs. abdomen advanced decay	-0.0534	0.510	1.2232	0.265
Cecum day 0 vs. cecum advanced decay	0.4624	0.001	7.4202	0.001

Table S6.

Results of nonparametric t-tests on levels of phylogenetic diversity between groups from mouse-model experiment 18S rRNA amplicon data set. Comparisons of diversity in decomposition-associated of microbial eukaryotic communities of soil, skin, and cecum, but not abdominal sites were significantly different from their starting community. Diversity levels between soil control types were different, but not between soils once decomposition advanced. P-values have been Bonferroni corrected for multiple comparisons.

Laboratory experiment, 18S							
Group1	Group2	G1 mean	G1 sd	G2 mean	G2 sd	t-stat	p
soil controls	soil with corpse	17.780	5.050	12.225	5.191	7.612	0.015
Soil controls	soil with corpse advanced decay	17.780	5.050	10.602	3.415	-10.613	0.015
desert soil control	forest soil control	12.067	2.839	19.725	4.981	6.749	0.015
desert soil control	grassland soil control	12.067	2.839	19.442	3.173	9.129	0.015
forest soil control	grassland soil control	19.725	4.981	19.442	3.173	-0.291	11.865
desert soil with corpse	forest soil with corpse	9.586	3.002	12.612	5.403	-2.693	0.240
desert soil with corpse	grassland soil with corpse	9.586	3.002	14.154	5.527	-4.047	0.015
forest soil with corpse	grassland soil with corpse	12.612	5.403	14.154	5.527	1.143	3.780
desert soil advanced decay	forest soil advanced decay	9.436	2.726	10.459	3.224	-1.191	3.750
desert soil advanced decay	grassland soil advanced decay	9.436	2.726	11.938	3.738	-2.739	0.105
forest soil advanced decay	grassland soil advanced decay	10.459	3.224	11.938	3.738	1.444	2.370
skin day 0	skin advanced decay	7.045	1.830	5.636	1.413	4.401	0.015
skin (body) advanced decay	skin (head) advanced decay	5.743	1.447	5.540	1.374	-0.833	5.775
abdomen day 0	abdomen advanced decay	7.159	0.203	6.710	1.452	-0.428	9.090
cecum day 0	cecum advanced decay	6.081	1.541	8.977	1.838	4.639	0.015

Table S7.

Results of ANOSIM and PERMANOVA tests on unweighted UniFrac distance matrix generated from 18S rRNA amplicon data sets of human model field experiments. All comparisons of decomposition-associated of microbial eukaryotic communities were significantly different from their starting community.

Field experiment February,18S				
Comparison	ANOSIM R	ANOSIM p-value	PERMANOVA Pseudo-F	PERMANOVA p-value
Soil controls vs. soil with corpse	-0.0092	0.588	32.0746	0.001
Soil controls vs. soil with corpse advanced decay	0.5988	0.001	45.3611	0.001
Skin day 0 vs. skin advanced decay	N/A	N/A	N/A	N/A
Soil advanced decay by sample location	0.3955	0.001	10.6966	0.001
Skin advanced decay by sample location	0.0364	0.071	1.3878	0.117
Field experiment April-18S				
Comparison	ANOSIM R	ANOSIM p-value	PERMANOVA Pseudo-F	PERMANOVA p-value
Soil controls vs. soil with corpse	0.0571	0.116	11.8605	0.001
Soil controls vs. soil with corpse advanced decay	0.1497	0.003	14.1942	0.001
Skin day 0 vs. skin advanced decay	NA	NA	NA	NA
Soil advanced decay by sample location	0.0849	0.001	2.2276	0.001
Skin advanced decay by sample location	-0.0038	0.598	1.2027	0.087

Table S8.

Results of nonparametric t-tests on levels of phylogenetic diversity between groups from 18S rRNA amplicon data sets of human-model field experiments. P-values have been Bonferroni corrected for multiple comparisons.

Field experiment Feb, 18S							
Group1	Group2	G1 mean	G1 sd	G2 mean	G2 sd	t-stat	p
soil controls	soil with corpse	27.025	3.613	17.353	10.148	8.916	0.007
soil controls	soil with corpse advanced decay	27.025	3.613	8.948	5.540	27.158	0.007
skin day 0	skin advanced decay	NA	NA	NA	NA	NA	NA
soil head	soil limb	8.518	4.185	13.412	7.093	-3.245	0.021
soil head	soil torso	8.518	4.185	7.210	4.108	1.446	1.246
soil limb	soil torso	13.412	7.093	7.210	4.108	-5.204	0.007
skin head	skin limb	NA	NA	5.341	1.753	NA	NA
skin head	skin torso	NA	NA	5.131	1.881	NA	NA
skin limb	skin torso	5.341	1.753	5.131	1.881	0.432	4.459
Field experiment April, 18S							
soil controls	soil with corpse	16.527	4.116	14.272	6.097	2.343	0.180
soil controls	soil with corpse advanced decay	16.527	4.116	12.782	5.133	4.502	0.009
skin day 0	skin advanced decay	7.758	1.246	6.551	3.485	0.488	5.733
soil head	soil limb	12.314	3.760	14.026	5.390	-1.346	1.683
soil head	soil torso	12.314	3.760	12.669	5.308	0.346	6.831
soil limb	soil torso	14.026	5.390	12.669	5.308	-1.148	2.331
skin head	skin limb	5.598	2.056	7.078	4.402	-1.695	0.999
skin head	skin torso	5.598	2.056	6.431	2.964	-1.396	1.674
skin limb	skin torso	7.078	4.402	6.431	2.964	1.198	2.097

Table S9.

Results of ANOSIM and PERMANOVA tests on Bray-Curtis distance matrix generated from ITS region amplicon data sets of mouse-model field experiments. All comparisons of decomposition-associated of microbial eukaryotic communities were significantly different from their starting community with the exception of the abdominal cavity.

Laboratory experiment, ITS				
Comparison	ANOSIM R	ANOSIM p-value	PERMANOVA Pseudo-F	PERMANOVA p-value
Soil controls vs. soil with corpse	0.1827	0.001	15.0776	0.001
Soil controls vs. soil with corpse advanced decay	0.2420	0.001	18.3682	0.001
soil controls by soil type	0.9928	0.001	37.1900	0.001
soils with corpse by soil type	0.6200	0.001	18.1846	0.001
soils with corpse advanced decay by soil type (no control soils)	0.5947	0.001	17.4416	0.001
Skin day 0 vs. skin advanced decay	NA	NA	NA	NA
Skin advanced decay by sample location	0.0538	0.003	1.9948	0.039
Abdomen day 0 vs. abdomen advanced decay	NA	NA	NA	NA
Cecum day 0 vs. cecum advanced decay	NA	NA	NA	NA

Table S10.

Results of nonparametric t-tests on levels of phylogenetic diversity between groups from mouse-model experiment ITS amplicon data set. P-values have been Bonferroni corrected for multiple comparisons.

.

Laboratory experiment, ITS							
Group1	Group2	G1 mean	G1 sd	G2 mean	G2 sd	t-stat	p
Soil controls	soil with corpse	122.705	30.833	76.775	37.065	7.952	0.015
Soil controls	soil with corpse advanced decay	122.705	30.833	62.468	24.703	-13.287	0.015
desert soil control	forest soil control	65.413	19.783	148.632	14.172	7.463	0.015
desert soil control	grassland soil control	65.413	19.783	99.392	16.260	2.679	0.360
forest soil control	grassland soil control	148.632	14.172	99.392	16.260	-11.206	0.015
desert soil with corpse	forest soil with corpse	44.794	11.576	106.641	34.442	-10.826	0.015
desert soil with corpse	grassland soil with corpse	44.794	11.576	66.927	24.028	-5.252	0.015
forest soil with corpse	grassland soil with corpse	106.641	34.442	66.927	24.028	-6.579	0.015
desert soil advanced decay	forest soil advanced decay	45.021	11.635	86.754	22.011	10.333	0.015
desert soil advanced decay	grassland soil advanced decay	45.021	11.635	54.385	54.385	-3.047	0.075
forest soil advanced decay	grassland soil advanced decay	86.754	22.011	54.385	54.385	7.180	0.015
skin day 0	skin advanced decay	NA	NA	NA	NA	NA	NA
skin (body) advanced decay	skin (head) advanced decay	44.271	22.801	44.156	19.089	0.032	14.655
abdomen day 0	abdomen advanced decay	NA	NA	NA	NA	NA	NA
cecum day 0	cecum advanced decay	NA	NA	NA	NA	NA	NA

Table S11.

Results of ANOSIM and PERMANOVA tests on Bray-Curtis distance matrix generated from ITS region amplicon data sets of human model field experiments. All comparisons of decomposition-associated of fungal communities were significantly different from their starting community with the exception of the abdominal cavity.

Field experiment February, ITS				
Comparison	ANOSIM R	ANOSIM p-value	PERMANOVA Pseudo-F	PERMANOVA p-value
Soil controls vs. soil with corpse	0.1053	0.001	47.7684	0.001
Soil controls vs. soil with corpse advanced decay	0.5923	0.001	63.1448	0.001
Skin day 0 vs. skin advanced decay	N/A	N/A	N/A	N/A
Soil advanced decay by sample location	0.1631	0.001	4.0009	0.001
Skin advanced decay by sample location	0.0079	0.296	0.8345	0.510
Field experiment April, ITS				
Comparison	ANOSIM R	ANOSIM p-value	PERMANOVA Pseudo-F	PERMANOVA p-value
Soil controls vs. soil with corpse	0.1741	0.001	22.314	0.001
Soil controls vs. soil with corpse advanced decay	0.2692	0.001	24.321	0.001
Skin day 0 vs. skin advanced decay	0.3512	0.129	4.6745	0.004

Table S12.

Results of nonparametric t-tests on levels of phylogenetic diversity between groups from ITS amplicon data sets of human-model field experiments. P-values have been Bonferroni corrected for multiple comparisons.

Field experiment Feb, ITS							
Group1	Group2	G1 mean	G1 sd	G2 mean	G2 sd	t-stat	p
soil controls	soil with corpse	142.008	24.512	98.702	35.446	11.319	0.007
soil controls	soil with corpse advanced decay	142.008	24.512	77.135	31.270	16.935	0.007
skin day 0	skin advanced decay	NA	NA	NA	NA	NA	NA
soil head	soil limb	64.450	29.783	105.240	32.346	-4.743	0.007
soil head	soil torso	64.450	29.783	73.377	24.903	-1.532	0.854
soil limb	soil torso	105.240	32.346	73.377	24.903	-4.786	0.007
skin head	skin limb	NA	NA	48.209	28.306	NA	NA
skin head	skin torso	NA	NA	39.683	30.361	NA	NA
skin limb	skin torso	48.209	28.306	39.683	30.361	0.892	2.590
Field experiment April, ITS							
soil controls	soil with corpse	115.058	26.084	102.846	29.760	2.424	0.180
soil controls	soil with corpse advanced decay	115.058	26.084	95.601	24.763	4.459	0.009
skin day 0	skin advanced decay	53.991	6.675	52.742	32.185	0.055	8.595
soil head	soil limb	94.875	13.879	103.789	23.689	-1.557	1.197
soil head	soil torso	94.875	13.879	94.357	26.060	0.095	8.361
soil limb	soil torso	103.789	23.689	94.357	26.060	-1.652	0.891
skin head	skin limb	50.396	23.457	59.553	35.345	-1.123	2.421
skin head	skin torso	50.396	23.457	48.654	30.822	0.247	7.164
skin limb	skin torso	59.553	35.345	48.654	30.822	2.093	0.288

Table S13.

Soil chemistry dynamics during decomposition: gravesoils relative to control soils. ANOVA results for comparisons between control soils and gravesoils at each timepoint for each soil type. *p*-value significance codes: *** 0.001, ** 0.01, * 0.05. Insufficient data: NA. In every case of significance, gravesoils had a higher value than the control soils. Soil chemistry data is plotted in Fig 4A, and raw data is available for download in excel table S18.

Measurement	Soil type	T0	T1	T2	T3	T4	T5	T6	T7
pH	Desert			***	NA	***	***	**	***
...	Forest	*	.	**	**	***	***	***	***
...	Shortgrass			***	*	***	***	***	*
C:N ratio	Desert	*		.	**	***	***	***	***
...	Forest		***	**	***	***	***	***	***
...	Shortgrass		*	***	***	***	**	***	***
Total C	Desert						.	*	
...	Forest								
...	Shortgrass		***				*		.
Total N	Desert	.			*	***	***	***	***
...	Forest			**	*	**	**	**	***
...	Shortgrass		***	.	*	***	**	**	**
ammonium	Desert	NA	***	*	**	***	***	***	***
...	Forest	NA	**	***	***	***	***	***	***
...	Shortgrass	NA	***	***	*	***	***	***	***
nitrate	Desert	NA	***		*	*	***		***
...	Forest	NA	*	.		**	*	**	
...	Shortgrass	NA			*	**			.

Table S14.

Levels at which we rarified data sets for statistical analyses. After sequence processing (described in methods), we had the following average sequences per sample for each experiment and marker type.

	mean sequences per sample (range)		
Experiment/analysis	16S rRNA	18S rRNA	ITS
laboratory (mouse)	90,768 (1,967-440,472)	28,780 (1,008-361,750)	171,277 (1,122-632,685)
field, February (human)	123,803 (2,205-705,134)	50,822 (1036-580,690)	86,162 (1,473-707,330)
field, April (human)	92,633 (1,009-306,691)	56,525 (1,038-446,279)	169,361 (1,480-2,408,583)
deep sequencing (16S) (all experiments)	1,272,147 (7,509-3,621,575)	N/A	N/A

Table S15.

Levels at which we rarified data sets for statistical analyses.

	Level of rarifying for downstream statistics		
Experiment/analysis	16S rRNA	18S rRNA	ITS
laboratory (mouse)	11,000	3,000	5,000
field, February (human)	20,000	3,000	5,400
field, April (human)	20,000	1,000	2,800
combined analyses	11,000	1,000	2500
deep sequencing (16S)	1,000,000	N/A	N/A

Table S16.

The soil source bacteria found by DBN analysis were found to be significantly (calculated as hypergeometric distribution, significant at a p-value <0.05) enriched for specific bacteria taxa, though the specific taxa differed by soil type.

.

Soil type		
forest	RB41	0
forest	Sphingomonadales	0
forest	Lactobacillales	0
forest	Rickettsiales	0.000552
forest	Clostridiales	0.004128
forest	Rhizobiales	0.009943
forest	Bacteroidales	0.020815
forest	Enterobacteriales	0.0212
forest	Burkholderiales	0.045969
desert	Acidobacteriales	0.012967
desert	Actinomycetales	0.016893
desert	Flavobacteriales	0.021628
desert	Erysipelotrichales	0.035782
desert	Turicibacterales	0.038704
shortgrass	RB41	0.001196538
shortgrass	Xanthomonadales	0.008120026
shortgrass	Pseudomonadales	0.011000972

Table S17.

Soil chemistry dynamics during decomposition: resampled gravesoils relative to control soils. ANOVA results for comparisons between control soils and resampled gravesoils at 10, 20, and 30 days after cadaver removal (at timepoints T1 and T5). *p*-value significance codes: *** 0.001, ** 0.01, * 0.05. Insufficient data: NA.

Measurement	Soil type	T1+10	T1+20	T1+30	T5+10	T5+20	T5+30
pH	Desert			**	***	***	***
...	Forest		**	*	***	***	***
...	Shortgrass				***	**	
C:N ratio	Desert	.	*	*	***	***	***
...	Forest		***	***	***	.	***
...	Shortgrass	***	***	***		*	**
Total C	Desert					.	
...	Forest				**	.	*
...	Shortgrass	***	**	**			
Total N	Desert	.	*	**		***	***
...	Forest						*
...	Shortgrass	***	***	***		**	*
Ammonium	Desert			***	***	***	***
...	Forest	*	***	***	***	***	***
...	Shortgrass	*	***	***	***	***	***
Nitrate	Desert	***	***	***	**	.	**
...	Forest		***			***	*
...	Shortgrass		**	**	.	*	***

Table S18.

Soil chemistry data is reported by sample in a downloadable excel sheet.

Table S19.

Nearest Sequenced Taxon Index scores for PICRUSt gene predictions are reported in a downloadable excel sheet.

Table S20.

We compared the proportion of decomposer OTUs detected in deeply sequenced day 1 potential source environments. Bar plots with error bars can be viewed in Fig 2B. We tested for significance using x is $p<0.05$ by Mann-Whitney U test.

		source comparisons		
decomposer community	experiment	ab vs. skin	ab vs. soil	skin vs. soil
abdominal	mouse, desert	x	x	
abdominal	mouse, short grass	x	x	
abdominal	mouse, forest		x	x
skin	mouse, desert	x	x	
skin	mouse, short grass	x	x	x
skin	mouse, forest		x	x
skin	human, winter	na	na	x
skin	human, spring	na	na	x
soil	mouse, desert	x	x	
soil	mouse, short grass	x	x	
soil	mouse, forest		x	x
soil	human, winter	na	na	x
soil	human, spring	na	na	x

References and Notes

1. J. A. Gilbert, J. D. Neufeld, Life in a world without microbes. *PLOS Biol.* **12**, e1002020 (2014). Medline doi:10.1371/journal.pbio.1002020

2. R. R. Parmenter, J. A. MacMahon, Carrion decomposition and nutrient cycling in a semiarid shrub-steppe ecosystem. *Ecol. Monogr.* **79**, 637–661 (2009). doi:10.1890/08-0972.1

3. M. Swift, O. Heal, J. Anderson, *Decomposition in Terrestrial Ecosystems* (Blackwell Scientific, Oxford, 1979).

4. J. C. Moore *et al*., Detritus, trophic dynamics and biodiversity. *Ecol. Lett.* **7**, 584 (2004).

5. D. O. Carter, D. Yellowlees, M. Tibbett, Cadaver decomposition in terrestrial ecosystems. *Naturwissenschaften* **94**, 12–24 (2007). Medline doi:10.1007/s00114-006-0159-1

6. P. S. Barton, in *Carrion Ecology, Evolution, and Their Applications*, M. E. Benbow, J. K. Tomberlin, A. M. Tarone, Eds. (CRC Press, 2015).

7. J. L. Metcalf, L. Wegener Parfrey, A. Gonzalez, C. L. Lauber, D. Knights, G. Ackermann, G. C. Humphrey, M. J. Gebert, W. Van Treuren, D. Berg-Lyons, K. Keepers, Y. Guo, J. Bullard, N. Fierer, D. O. Carter, R. Knight, A microbial clock provides an accurate estimate of the postmortem interval in a mouse model system. *eLife* **2**, e01104 (2013). Medline doi:10.7554/eLife.01104

8. J. L. Pechal, T. L. Crippen, M. E. Benbow, A. M. Tarone, S. Dowd, J. K. Tomberlin, The potential use of bacterial community succession in forensics as described by high throughput metagenomic sequencing. *Int. J. Legal Med.* **128**, 193–205 (2014). Medline

9. E. R. Hyde, D. P. Haarmann, J. F. Petrosino, A. M. Lynne, S. R. Bucheli, Initial insights into bacterial succession during human decomposition. *Int. J. Legal Med.* **129**, 661–671 (2015). Medline doi:10.1007/s00414-014-1128-4

10. W. E. D. Evans, *The Chemistry of Death* (Charles C Thomas, Springfield, IL, 1963).

11. M. G. I. Langille, J. Zaneveld, J. G. Caporaso, D. McDonald, D. Knights, J. A. Reyes, J. C. Clemente, D. E. Burkepile, R. L. Vega Thurber, R. Knight, R. G. Beiko, C. Huttenhower, Predictive functional profiling of microbial communities using 16S rRNA marker gene sequences. *Nat. Biotechnol.* **31**, 814–821 (2013). Medline doi:10.1038/nbt.2676

12. D. Houston, in *Neotropical Ornithology* (American Ornithologists' Union Monograph No. 36, Washington, DC, 1985), pp. 856–864.

13. M. Kaspari, M. N. Garcia, K. E. Harms, M. Santana, S. J. Wright, J. B. Yavitt, Multiple nutrients limit litterfall and decomposition in a tropical forest. *Ecol. Lett.* **11**, 35–43 (2008). Medline

14. P. S. Barton, S. A. Cunningham, D. B. Lindenmayer, A. D. Manning, The role of carrion in maintaining biodiversity and ecological processes in terrestrial ecosystems. *Oecologia* **171**, 761–772 (2013). Medline doi:10.1007/s00442-012-2460-3

15. J. Amendt, C. P. Campobasso, E. Gaudry, C. Reiter, H. N. LeBlanc, M. J. R. Hall, Best practice in forensic entomology—Standards and guidelines. *Int. J. Legal Med.* **121**, 90–104 (2007). Medline doi:10.1007/s00414-006-0086-x

16. J. G. Caporaso, C. L. Lauber, W. A. Walters, D. Berg-Lyons, C. A. Lozupone, P. J. Turnbaugh, N. Fierer, R. Knight, Global patterns of 16S rRNA diversity at a depth of millions of sequences per sample. *Proc. Natl. Acad. Sci. U.S.A.* **108** (suppl. 1), 4516–4522 (2011). Medline doi:10.1073/pnas.1000080107

17. S. T. Bates, J. C. Clemente, G. E. Flores, W. A. Walters, L. W. Parfrey, R. Knight, N. Fierer, Global biogeography of highly diverse protistan communities in soil. *ISME J.* **7**, 652–659 (2013). Medline doi:10.1038/ismej.2012.147

18. K. L. McGuire, S. G. Payne, M. I. Palmer, C. M. Gillikin, D. Keefe, S. J. Kim, S. M. Gedallovich, J. Discenza, R. Rangamannar, J. A. Koshner, A. L. Massmann, G. Orazi, A. Essene, J. W. Leff, N. Fierer, Digging the New York City skyline: Soil fungal communities in green roofs and city parks. *PLOS ONE* **8**, e58020 (2013). Medline

19. J. G. Caporaso, J. Kuczynski, J. Stombaugh, K. Bittinger, F. D. Bushman, E. K. Costello, N. Fierer, A. G. Peña, J. K. Goodrich, J. I. Gordon, G. A. Huttley, S. T. Kelley, D. Knights, J. E. Koenig, R. E. Ley, C. A. Lozupone, D. McDonald, B. D. Muegge, M. Pirrung, J. Reeder, J. R. Sevinsky, P. J. Turnbaugh, W. A. Walters, J. Widmann, T. Yatsunenko, J. Zaneveld, R. Knight, QIIME allows analysis of high-throughput community sequencing data. *Nat. Methods* **7**, 335–336 (2010). Medline doi:10.1038/nmeth.f.303

20. N. A. Bokulich, S. Subramanian, J. J. Faith, D. Gevers, J. I. Gordon, R. Knight, D. A. Mills, J. G. Caporaso, Quality-filtering vastly improves diversity estimates from Illumina amplicon sequencing. *Nat. Methods* **10**, 57–59 (2013). Medline doi:10.1038/nmeth.2276

21. E. Pruesse, C. Quast, K. Knittel, B. M. Fuchs, W. Ludwig, J. Peplies, F. O. Glöckner, SILVA: A comprehensive online resource for quality checked and aligned ribosomal RNA sequence data compatible with ARB. *Nucleic Acids Res.* **35**, 7188–7196 (2007). Medline doi:10.1093/nar/gkm864

22. J. G. Caporaso, K. Bittinger, F. D. Bushman, T. Z. DeSantis, G. L. Andersen, R. Knight, PyNAST: A flexible tool for aligning sequences to a template alignment. *Bioinformatics* **26**, 266–267 (2010). Medline doi:10.1093/bioinformatics/btp636

23. V. A. Smith, J. Yu, T. V. Smulders, A. J. Hartemink, E. D. Jarvis, Computational inference of neural information flow networks. *PLOS Comput. Biol.* **2**, e161 (2006). Medline doi:10.1371/journal.pcbi.0020161

24. M. I. Love, W. Huber, S. Anders, Moderated estimation of fold change and dispersion for RNA-seq data with DESeq2. *Genome Biol.* **15**, 550 (2014). Medline doi:10.1186/s13059-014-0550-8

25. P. J. McMurdie, S. Holmes, Waste not, want not: Why rarefying microbiome data is inadmissible. *PLOS Comput. Biol.* **10**, e1003531 (2014). Medline doi:10.1371/journal.pcbi.1003531

26. S. Weiss, D. O. Carter, J. L. Metcalf, R. Knight, Carcass mass has little influence on the structure of gravesoil microbial communities. *Int. J. Legal Med.* 10.1007/s00414-015-1206-2 (2015). Medline doi:10.1007/s00414-015-1206-2

27. D. O. Carter, J. L. Metcalf, A. Bibat, R. Knight, Seasonal variation of postmortem microbial communities. *Forensic Sci. Med. Pathol.* **11**, 202–207 (2015). Medline doi:10.1007/s12024-015-9667-7

28. C. L. Lauber, M. Hamady, R. Knight, N. Fierer, Pyrosequencing-based assessment of soil pH as a predictor of soil bacterial community structure at the continental scale. *Appl. Environ. Microbiol.* **75**, 5111–5120 (2009). Medline doi:10.1128/AEM.00335-09

29. E. A. Dinsdale, R. A. Edwards, D. Hall, F. Angly, M. Breitbart, J. M. Brulc, M. Furlan, C. Desnues, M. Haynes, L. Li, L. McDaniel, M. A. Moran, K. E. Nelson, C. Nilsson, R. Olson, J. Paul, B. R. Brito, Y. Ruan, B. K. Swan, R. Stevens, D. L. Valentine, R. V. Thurber, L. Wegley, B. A. White, F. Rohwer, Functional metagenomic profiling of nine biomes. *Nature* **452**, 629–632 (2008). Medline